Degree Project in Technology

First Cycle, 15 credits

Cosmic Lighthouse: Exploring X-ray Pulsars in Python

AMER AVDIC, ALFRED MJÖRNHEIM

Theoretical Physics

Cosmic Lighthouse: Exploring X-ray Pulsars in Python

Amer Avdic and Alfred Mjörnheim
SA114X Degree Project in Engineering Physics, First Level
Department of Physics
Royal Institute of Technology (KTH) [1]

June 7, 2024

[1]Supervisors: Inga Saathoff and Sophie Rosu

Abstract

A supernova explosion of a massive star at the end of its life leaves behind a compact object, either a black hole or a neutron star. We study a particular aspect of neutron stars in this project. A neutron star is a fast spinning, extremely dense object with a strong magnetic field. Neutron stars can emit light beams from their magnetic poles. For an observer on Earth these beams appear as pulses of light since the neutron stars rotation axis is not aligned with the magnetic axis. These pulses of light are practically the only way to gather information about neutron stars which are otherwise difficult to observe. We study the binary system Centaurus X−3 (Cen X−3) with an accretion powered x-ray emitting pulsar. We use a model of a neutron star showing how the pulses of radiation appear from Earth, based on a set of chosen parameter values. These parameters gather information regarding the geometry of the neutron star, its mass and radius, as well as some properties related to the way the radiation is emitted. We use a particle swarm optimization method to fit the observed light pulse of the Cen X−3 system. Our resulting fits do not converge to a single solution, rather it shows that there are many possible configurations reproducing the observed light pulses. This shows that while our model can be used to simulate the behavior of neutron stars it requires further development if one wishes to obtain reliable estimates for the neutron stars paremeters.

Sammanfattning

En supernovaexplosion av en massiv stjärna i slutet av dess liv lämnar efter sig ett kompakt objekt, antingen ett svart hål eller en neutronstjärna. Vi studerar en viss aspekt av neutronstjärnor i detta projekt. En neutronstjärna är ett snabbt roterande objekt med extremt hög densitet och starkt magnetiskt fält. Neutronstjärnor kan avge strålning från sina magnetiska poler. Som följd av att den magnetiska axeln och rotations axeln inte är i linje med varandra framstår strålningen för en observatör på jorden som korta ljuspulser. Dessa ljuspulser är närapå det enda sättet att samla information om neutronstjärnor som annars är svåra att observera. Vi använder en modell av en neutronstjärna som visar hur strålningspulserna framstår från jorden baserat på ett set av valda parameter värden. Dessa parametrar innehåller information om neutronstjärnans geometri, dess massa och radie, samt några egenskaper relaterade till hur strålningen emitteras. Vi använder också en partikelsvärm optimering för att passa den simulerade pulsen till den observerade pulsen från Cen X−3. Våra resulterande passningar konvergerar inte till en specifik lösning, utan visar snarare att det finns många möjliga konfigurationer som reproducerar de observerade ljuspulserna. Detta visar att medan vår modell kan användas för att simulera beteendet hos neutronstjärnor så krävs det ytterligare utveckling av modellen för tillförlitliga parameteruppskattningar.

Contents

Chapter 1

Introduction and astrophysical background

The aim of this project is to investigate how different properties of a neutron star affect its light emissions and to determine possible configurations of these properties for the Centaurus X−3 neutron star pulsar. In order to do this, we modified a toy model of a pulsar written in python and developed by I. Saathoff which for a given set of parameter values simulates the emitted radiation. A particle swarm optimization method is employed to fit the simulated radiation to observed radiation. In Chapter 1 we provide an introduction to neutron star pulsars, especially how they form, and provide the relevant astrophysical context necessary to understand this thesis. In Chapter 2 we describe how the emissions are modeled and introduce the optimization methods. In Chapter 3 we present the resulting fits for different study cases and discuss them in regard of the limitations of our model. In Chapter 4 we provide our conclusions and discuss suggestions toward the improvement of our method as well as further research in this field.

1.1 How a neutron star is formed

Neutron stars make up one of a few possible endpoints in a star's lifecycle. We here provide a brief description of the evolution of a star leading up to a neutron star. Star formation starts when a gas cloud with a mass exceeding the Jeans mass [1] collapses under its own gravity and accretes mass from its surroundings, forming proto-stars. Due to turbulent flows within the gas cloud, the newly formed stars will typically have an initial rotation speed around their rotation axis. The conservation of angular momentum causes this rotation to persist throughout the entire lifecycle of the stars [2]. The turbulent flows in the gas cloud cause movement of charged particles which in combination with the magnetic fields already belonging to the cloud gives stars their magnetic fields [3]. The formation of a main-sequence star means that the newly formed proto-star has become dense enough to create the necessary conditions for hydrogen fusion to start inside its core. A star remains in the main-sequence as long as it has sufficient hydrogen to fuse in its core. The duration of this period is inversely proportional to the mass of the star raised to the power 2.5, which means that higher mass stars have significantly reduced lifespans [4, 5]. Stars of mass larger than $0.4M_{\odot}$ see their core beginning to collapse by the end of the main-sequence phase since no fusion is balancing their own gravity; however as it shrinks the pressure builds up. Simultaneously hydrogen in a layer

Progenitor star mass ($M_\odot$)	Progenitor star metallicity	Compact Object
9-10	any	Neutron star
10-25	any	Neutron star
25-40	lower than or solar	Black hole after fallback
25-40	higher than solar	Neutron star
≥ 40	lower than solar	Black hole
≥ 40	solar	Black hole after fallback
≥ 40	higher than solar	Neutron star

Table 1.1: Compact object (neutron star or black hole) left after a supernova explosion depending on the progenitor star's mass and metallicity. Black hole after fallback refers to the edge case scenario where the compact object initially is a neutron star but it pulls in material that was ejected during the supernova turning it into a black hole. The table was made using data from [7]

.

just outside the core of the star begins to fuse, causing the star to swell and the core to further contract. When the pressure is high enough in the core, helium fusion starts in the core. The star now enters a giant or supergiant phase. The next phases of evolution depend on the mass of the star [6].

Intermediate mass stars ($0.4M_\odot \lesssim M \lesssim 8M_\odot$)**:** Right before the end of the final giant phase these stars form an inert core of carbon thus fusion of H and He only occurs in the shells. Strong stellar winds disgorge the outer layers,: while the core collapses into a degenerate matter star called a white dwarf. This process is known as a planetary nebula [6]. Degenerate matter can only support a star of mass up to the Chandrasekhar limit of $\sim 1.4M_\odot$ [2].

Massive stars ($M \gtrsim 8M_\odot$) : Massive stars possess the capacity to generate sufficient pressure and temperature to initiate fusion within a carbon core, which remains dormant in smaller stars. This creates an inner core of neon which in turn fuses its innermost parts into oxygen and so on and so forth until iron fusion. The result of the repeated fusion is a core consisting of concentric layers of increasingly heavier elements as seen in Figure 1.1. As fusion of iron is an endothermic process fusion drops when iron is formed. With no further fusion pressure to support the mass of the star, the core collapses and turns into degenerate matter, forming a neutron star or black hole while the outer layers are vehemently expelled into the interstellar medium. This sequence of events is called a supernova explosion [2]. Several factors determine if the end product is a neutron star or a black hole: the main two are the progenitor mass and its metallicity. A high mass increases the probability of forming a black hole, while a high metallicity favors neutron star formation, see Table 1.1 for details.

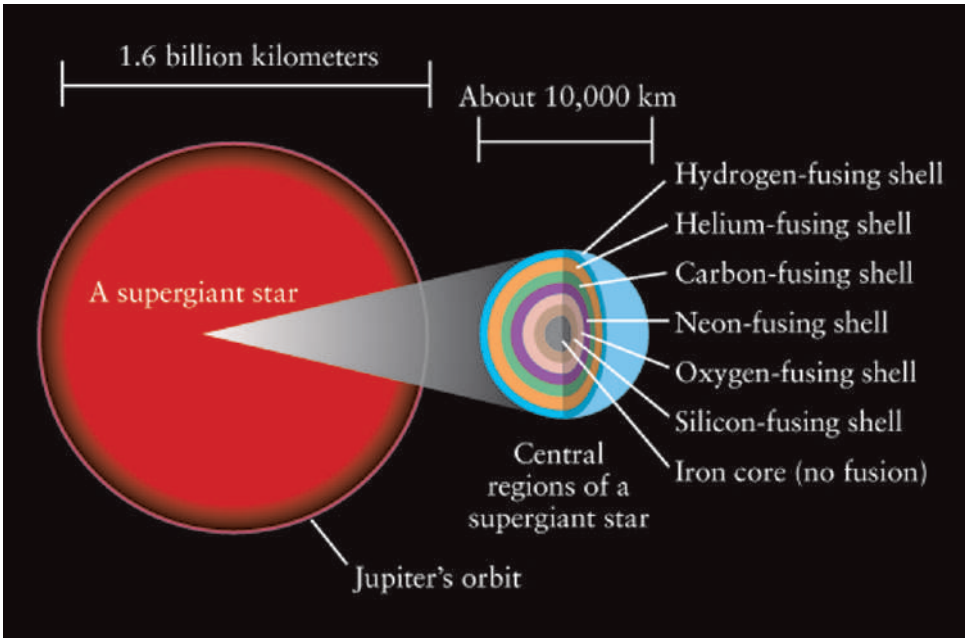

Figure 1.1: Schematic picture of the core of a massive star right before a supernova explosion. Scales are only approximately true and may vary between stars. ©University of Alberta

.

1.2 Properties of neutron stars

1.2.1 Neutron star structure

A neutron star is typically divided into five concentric regions of increasing density from the exterior to the interior: atmosphere, outer crust, inner crust, outer core, and inner core (see Figure 1.2).

Atmosphere/surface layers: The surface layers are defined as the layers of density lower than $\sim 10^9$ kg m^{-3} and consist of tightly packed atomic polymers of iron. This matter has a uni-dimensional behavior with high conductivity parallel to the magnetic field but virtually zero in all perpendicular directions.

Outer crust: The outer crust has a density ranging from $\sim 10^9$ kg m^{-3} to $\sim 4.3 \times 10^{14}$ kg m^{-3}. It is composed of heavy nuclei (typically iron) that due to Coulomb forces between protons within the nuclei form a regular repeating pattern, that is to say, a Coulomb lattice. This lattice structure lies within a gas of electrons moving at relativistic speeds. Due to the high gravitational pressure in the outer crust these electrons are packed so densely that they enter a degenerate state.

Inner crust: The density of the inner crust is approximately within the range 4.3×10^{14} kg m^{-3} $\lesssim \rho \lesssim 2 \times 10^{17}$ kg m^{-3}. Like the outer crust this area is filled with a lattice of nuclei in a degenerate electron gas. However, due to neutronization, a process turning a proton and an electron into a neutron, these nuclei are very rich in neutrons. The inner crust also contains free degenerate neutrons. In the innermost parts nuclei

start to break apart thus releasing the neutrons and creating a degenerate neutron gas, usually called neutron fluid.

Outer core: The outer core of a neutron star is almost entirely made of this neutron fluid with a small amount of protons and electrons. The density of the outer core is larger than $\sim 2 \times 10^{17}$ kg m^{-3}. Since neutrons are fermions they obey the Pauli exclusion principle, that is to say, two neutrons cannot occupy the same quantum state simultaneously. When the neutrons become densely packed many neutrons are forced to enter higher energy states. The higher energy states then create a pressure that is balancing gravity to keep the neutron star from collapsing onto itself.

Inner core: The inner core is the very innermost part of a neutron star and there is no consensus regarding its structure or even existence. We here discuss the most popular theories. The first theory states that there is no real inner core; it is simply made up of the same neutron liquid as the outer core [4]. There are models/simulations of neutron stars implementing this type of core without resulting in the star collapsing under its own gravity [4]. Another theory states that the inner core consists of hyperons, which are baryons composed of three quarks, one up (u), one down (d), and one strange (s) [4]. Since s quarks have a larger mass than u and d quarks the resulting hyperons are more massive than protons and neutrons. A third theory states that the core is made of Bose-Einstein condensates [4]. Bose-Einstein condensates are made up of either pions, which are mesons made up of a quark-antiquark pair of either u or d, or of kaons which are like pions but with a s antiquark instead of u or d antiquarks. If very extreme density and temperature conditions are present neutrons and protons can dissolve into quarks and form what we call a plasma of quarks. In a quark plasma the quarks can move freely and are not confined by the structure of hadrons. This means more quarks can fit in a smaller area and therefore the latter have very high densities. [4].

1.2.2 Neutron star radiation - pulsars

The existence of neutron stars was first suggested in 1934 by Walter Baade and Fritz Zwicky. They were however not observed until 1967 during a search for quasars, a type of galaxy emitting radio waves. During that night in 1967 the Irish astrophysicist Jocelyn Bell Burnell and the British radio astronomer Anthony Hewish detected 20 ms-long radio pulses appearing regularly every 1.337 seconds. After ruling out human interference, and interstellar lifeforms, they concluded that it should be a compact faraway object emitting pulses of radiation. Additional objects similar to these have since been discovered, and they have been coined 'pulsars', for 'pulsating radio sources'. It is important to note, however, that not all pulsars emit radio waves [2]. Later these pulsars were found to be rotating neutron stars emitting radiation from their magnetic poles. The appearance of short pulses rather than a constant beam of radiation stems from a misalignment between the magnetic axis and the rotational axis of the neutron star. The angle between these axes is called the magnetic colatitude (see Figure 1.3). Pulsars are commonly categorized after their source of power:

- Rotation powered: The magnetic field of a rotating pulsar induces an electric field, which according to Lenz's law slows down the rotation speed. The decreasing

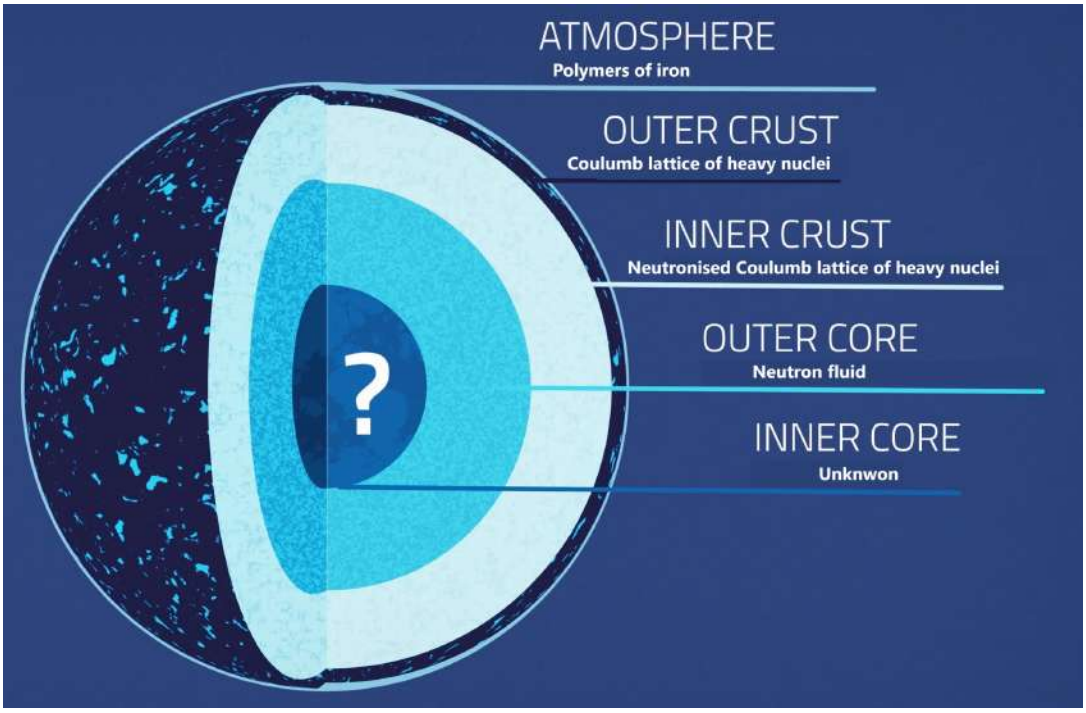

Figure 1.2: Schematic pictureof the different layers of a neutron star (not to scale). Modified from ©Nasa

.

rotational energy is then released in the form of radiation. The first discovered pulsar as well as millisecond pulsars are included in this category [8].

- Accretion powered: A pulsar powered by the gravitational potential energy of accreting matter being pulled in to the star. These pulsars are found in binary systems since they need another star to draw mass from, and most often emit X-ray radiation. The neutron star we study in this project, Centaurus X−3 (Cen X−3) belongs to this category [9].

- Internal energy powered: A pulsar using the decay of internal energy as its power source. The internal energy comes from very strong magnetic fields in the case of a magnetar or in other cases leftover heat energy from the supernova [10].

1.3 Gravitational light bending

The general theory of relativity (GR) describes gravity as the result of spacetime being warped around massive objects in accordance with Einstein's field equation [11]. Nearby objects follow the curvature of spacetime causing masses to accelerate towards each other, similar to how Newtonian mechanics describe gravitational attraction. A key difference with the GR framework is that even massless particles such as photons follow spacetime curvatures, so light will travel along a geodesic instead of a straight line. This phenomenon is called gravitational light bending, an illustration of it is provided in Figure 1.4. A geodesic is the shortest path around the surface of a curved object [11]. The concept of gravitational light bending is quite critical for our purposes, since the radiation

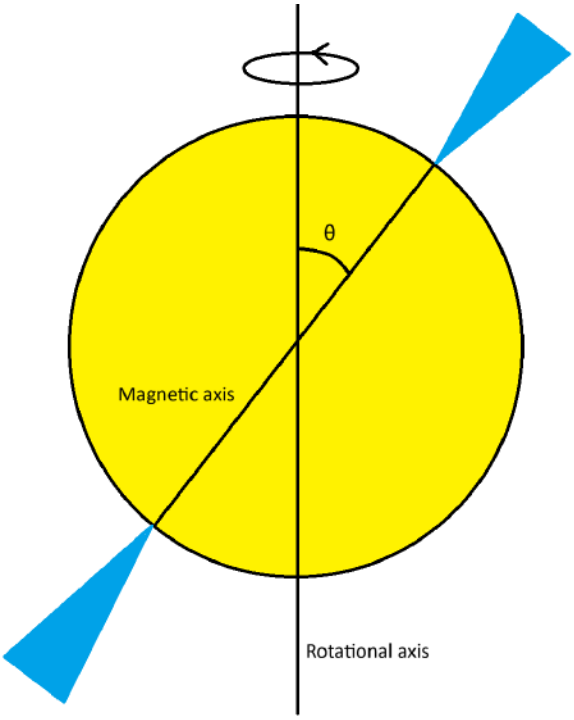

Figure 1.3: Schematic picture of a neutron star and its rotational and magnetic axes. The angle between the two axes, the magnetic colatitude, is denoted by θ.

emitted from the neutron star will bend due to the gravity of the neutron star itself. To calculate how much the light bends there is an exact method although this method involves solving elliptical integrals [12] which has to be done numerically and demand somewhat substantial computational costs. Instead we here use an approximate formula valid for objects with a radius at least twice as large as the Schwarzschild radius that was derived in [12]. A neutron star's radius is typically three times the Schwarzschild radius, hence the formula is valid for our purposes. The formula for this approximation is:

$$1 - \cos\alpha = (1 - \cos\phi)(1 - r_g/R), \tag{1.1}$$

where α denotes the emission angle as seen by an observer located at the emission point, ϕ is the azimuthal angle, r_g is the Schwarzschild radius, and R is the radius of the neutron star.

1.4 Centaurus X−3

Centaurus X−3 is a binary system consisting of the Cen X−3 neutron star and its companion Krzeminski's star, an O-type supergiant. The neutron star itself has a spin period of $\sim$4.8 seconds and is an accretion powered X-ray emitting pulsar [14]. There have been large fluctuations in the X-ray radiation from this system with no widely accepted reason as to what causes this. The dataset we used is based on measurements taken during a timespan much smaller than the period of each fluctuation, hence the fluctuations should not affect our results [15]. Krzeminski's star has a mass of $20.5 \pm 0.7 M_\odot$ and a radius of $12 R_\odot$ whereas the neutron star has a mass of $1.21 \pm 0.21 M_\odot$ [16]. There are

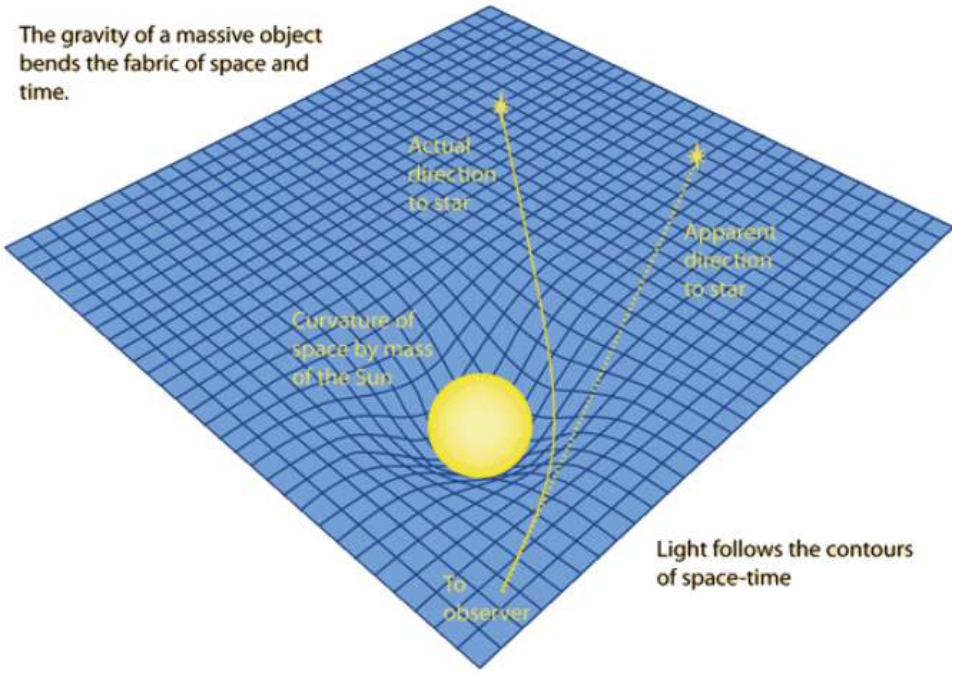

Figure 1.4: Illustration of gravitational light bending, in this case around the sun. The effect is amplified for illustrative purposes and neither sizes nor lengths are to scale. The picture is from [13].

currently no reliable ways to accurately measure the radius of a neutron star, mainly because measuring the distance to the neutron star comes with large uncertainties which carry over to radii measurements [15]. Nonetheless the current research indicates all neutron stars should have radii between 9 and 13 km [15].

Chapter 2

Model and fitting methodology

The problem studied in this thesis involves observational data from two single-pole pulse profiles, each originating from one of the poles of a neutron star [15]. The goal of this project is to study which values of the parameters of the X-ray pulsar model could explain the observations.

To do this, we simulated a beampattern. A pulsar's beampattern is the X-ray emission intensity from the pulsar. It is a function of the position on the star's surface. We assumed a basic model where the beampattern plot is a simple 2D cosine plot projected on the spherical plane. More specifically, the beampattern is defined by the following equation:

$$f(\alpha, \phi, \delta_\alpha, \delta_\phi, \gamma) = [(\cos\alpha + \delta_\alpha)(\cos\phi + \delta_\phi)]^\gamma, \tag{2.1}$$

In equation (2.1), where α and ϕ represent coordinates on the angle plane going from $-\pi/2$ to $\pi/2$, δ_α and δ_ϕ represent shifts from a particular position on the plane going from $-\pi$ to π, and γ represents the sharpness of the beampattern's peak.

We also assume that the properties of the neutron star are determined by the following parameters: the orientation of the neutron star's rotational axis, the magnetic colatitude, the beampattern's power and location on the surface of the neutron star, the relative phase shift of the neutron star's rotation, and the neutron star's mass and radius. The latter two variables also allowed for the effects of gravitational light bending to be studied (see Sections 3.2 and 3.3.2). In particular, we studied the importance of this phenomenon as a function of the mass-radius ratio of the star. Equation (1.1) was taken into account while doing this. The exact parameters we used other than the neutron star's mass and radius will be presented in Section 2.1. The effect of the parameters can be seen in the example images presented in Section 2.2.

When examining the behavior of a pulsar the most important tool is arguably the pulse profile. A pulse profile is the measured intensity of radiation from the pulsar over the course of two periods of revolution (see Figure 2.1). For our simulations we however used a modified pulse profile showing only one period since it provides better readability and contains all necessary information. We used the pulse profile obtained by [15]. We simulated pulse profiles for Cen X−3 for a given set of parameter values and tweaked those values in order to match the measurements, the process is described more in depth in following sections.

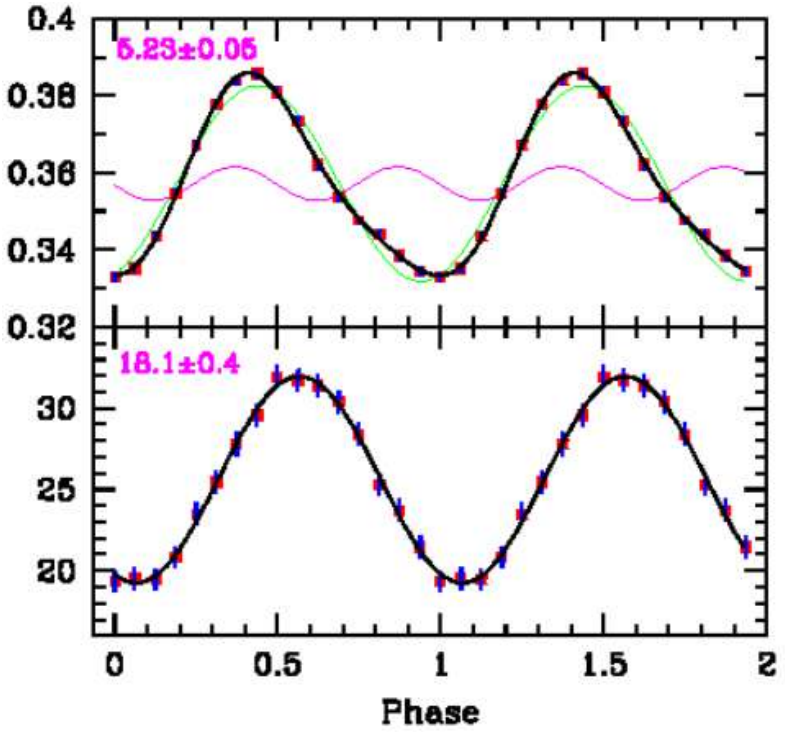

Figure 2.1: Pulse profiles of an accreting millisecond pulsar showing the relative intensity as a function of the phase. [17]

2.1 Simulation

We derived the properties of Cen X−3 with the help of optimization (see Section 2.3). The results obtained were then visualized with the help of three plots. These plots simulated various characteristics of the neutron star, with example images shown in Section 2.2. The left plot in Figure 2.2 is used in order to simulate the motion of the neutron star with respect to an observer located on Earth. The middle plot in Figure 2.2 is used with the intent to simulate the beampattern, its intensity and its location relative to the observer. The right plot in Figure 2.2 serves to compare a simulated pulse profile with a profile obtained from the X-ray pulsar. The combined information about the star's rotation and the beampattern from the previous two plots serve to visualize the profile being simulated in this plot. As such, the simulated profile is based on how the neutron star's parameters were set for the previous two plots.

Specifically, the first plot shows the orientation of the rotational axis with the help of two variables: the rotation inclination, which is the rotation axis' angle to the horizontal equator (see Figure 2.3), and the rotation azimuth, which is the angle from the vertical equator (see Figure 2.3). It also includes yellow and pink dots, which represent emission regions on the surface of the neutron star. This is where the beampattern is being observed, for a certain phase in the star's rotation. As such, the yellow and pink dots will henceforth collectively be referred to as observation points. The magnetic colatitude is the angle between the rotation and magnetic axes, as introduced in Section 1.2.2. In the context of neutron star rotation, we define a reference point on the celestial sphere that corresponds to the zero phase of the star's rotation. This point is represented by a pink

dot and is located along a specific meridian line determined by the azimuth angle of the star's rotational axis. This azimuth angle, measured in the plane perpendicular to the line of sight, serves as the initial reference for the phase of the neutron star's rotation. In other words, the relative phase shift of the star's rotation is set to 0 at that meridian line.

The second plot shows a spherical angle plane as the base of the plot which represents points on the surface of the star. The axis perpendicular to the plane shows the radiation intensity as a function of the position on the surface of the star. The plot includes a simulated beampattern with varying intensity, in other words the beampattern power. The location of the beampattern is fixed by the azimuth and inclination. Also included are the observation points from the previous plot. These are now projected onto the base plane where they simulate a pulse profile based on their proximity to the simulated beampattern. The red dots represent the actually observed, post-gravitational light bending, beam intensity as a function of position on the surface of the star. They are henceforth referred to as the measured data. The green dots represent the calculated, pre-gravitational light bending beam intensity as a function of position, henceforth referred to as the intrinsic data. The calculations are based on the measured data. For an illustration of the above parameters, see Figure 2.3.

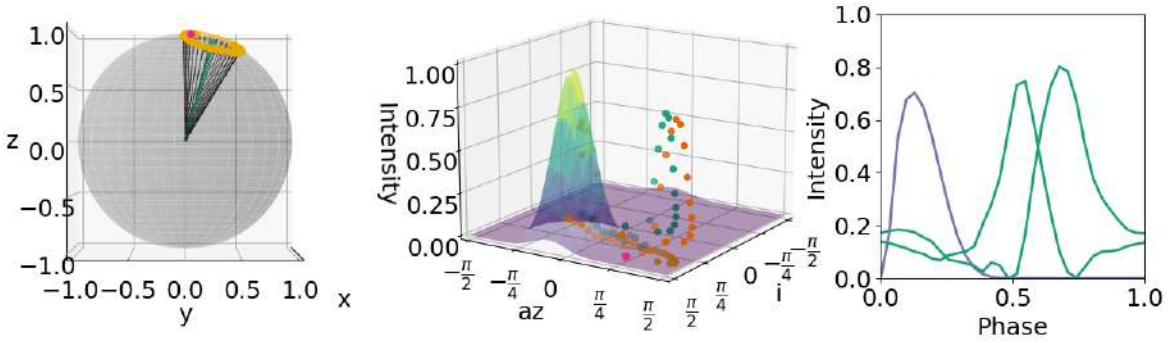

Figure 2.2: Example of plots used to study X-ray pulses and the neutron star emitting them. Left panel: Geometry of the system. The green line shows the position of the spin axis, while the pink/yellow points show the position of the emission region during the rotation of the star. Middle panel: Beampattern of the system. The actual beampattern is represented with a 3D curve, and the plane at the base of the plot is a projection of points on the surface of the star. Also shown are the emission regions from the left plot, measured beampattern data (red dots) and the same data when gravitational light bending is not taken into account (green dots). The emission regions being close to the beampattern in this plot corresponds to the emission regions being close to the beampattern on the first plot. Right panel: Pulse profiles. The measured pulse profiles from each pole are shown with green curves. The red curve (shown as purple in later plots) represents a simulated pulse profile that is based on how the two previous plots were configured. In general, the closer the emission regions are to the beampattern in the middle plot, the higher the overall intensity of the simulated pulse profile is in this plot.

We note that the intensity shown in the intrinsic data does not follow the intensity of the simulated beampattern unlike the observation points. This is because these data

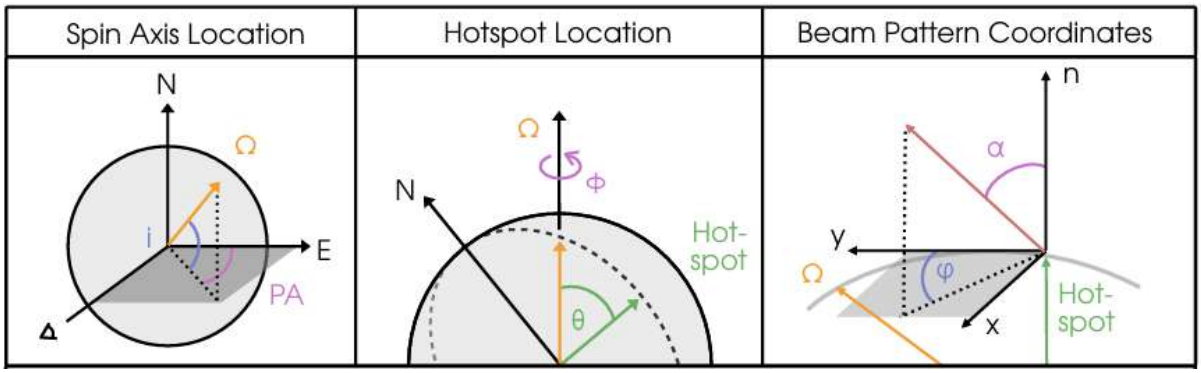

Figure 2.3: Illustration of the angular parameters defined for the neutron star. Left panel: The vector Ω represents the rotational axis, i represents the rotation inclination, the position angle (PA) represents the rotation azimuth, the N-E plane is the plane of the vertical equator, and the plane perpendicular to the N-E plane is the plane of the horizontal equator. Middle panel: The angle θ between the rotational axis and the emission region, called 'hotspot' in the figure, is the magnetic colatitude. The circular vector Φ that goes around the rotational axis represents the relative phase of the star's rotation. Right panel: α is the rotational inclination and φ is the rotation azimuth. Figure taken from [15].

represent the true location and intensity of the beampattern as a result of being based on real data. The observation points also do not take gravitational light bending into account since they represent points on the surface of the neutron star, where the light has not traveled far enough away from the star for such a gravitational effect to be significant. So if the intrinsic data and observation points were to be aligned close to each other, hypothetically, it would lead to a simulated curve that would fit one of the measured pulse profiles in the third plot.

The third plot shows the beampattern intensity as a function of the phase, where each measured phase point is matched with an emission region from the previous plots. In other words, this plot is a pulse profile plot. The green curves are the actual pulse profiles measured for each pole. The purple curve is the simulated one.

We find it important to mention that, for simplicity's sake, we have ignored any potential asymmetry in the beampattern other than the shift in its azimuth and inclination. That, however, does not necessarily mean that the beampattern will only have one source of asymmetry. This is if one follows the assumption that the magnetic poles of a star are not always antipodal to each other [15], which is the assumption under which we are working here.

2.2 Particular cases

In this section, we present five particular cases to illustrate how the pulse profiles introduced in Figure 2.2 are affected by a change in the various parameters introduced in Section 2.1. The parameters of the different cases are summarized in Table 2.1.

Case 1 (see Figure 2.4): In this case, the magnetic colatitude and the pink dot

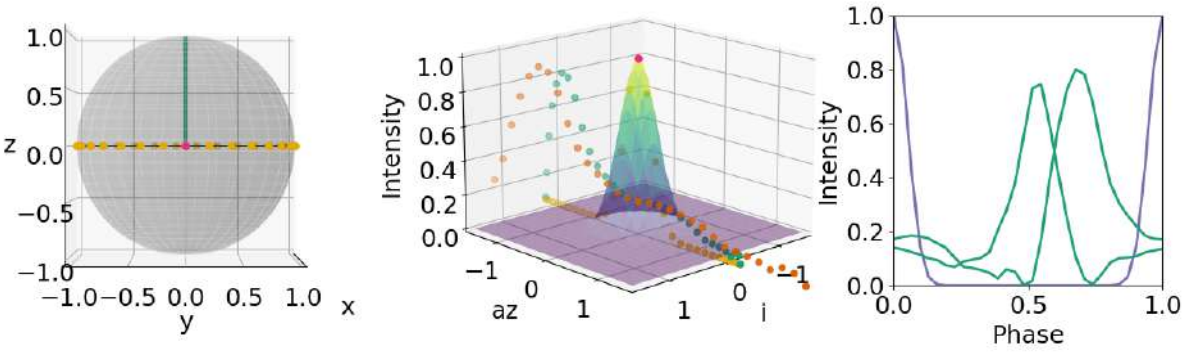

Figure 2.4: Pulse profile plots, as in Figure 2.2, but for Case 1. The parameters are listed in Table 2.1.

are at the tip of the beampattern in plot 2. It corresponds to a pulse profile in plot 3 that peaks for phases near phase 0, in other words for observation points near in phase to the pink dot in plot 2. The beampattern has its azimuth and inclination values set to approximately 0 in plot 2; that corresponds to a beampattern pointing roughly to the observer's direction in plot 1.

Case 2 (see Figure 2.5): In this case, as in the previous case, the beampattern is pointing toward the observer. But due to the rotation axis also pointing in that direction and the 90° magnetic colatitude, none of the observation points pass through the beampattern, resulting in no recorded intensity in plot 3.

Case 3 (see Figure 2.6): In this case, the magnetic colatitude is 0°, and the beampattern location is where the rotational axis points to in plot 1. As a result, the beampattern does not rotate around the star and it is always observed at maximum intensity, resulting in a pulse profile whose intensity is constantly 1.

Case 4 (see Figure 2.7): This case is similar to Case 1, with the difference being that the pink dot is fully behind the star from our point of view instead of in front of the star. As a result, the pulse profile records a peak for a phase near 0.5.

Case 5 (see Figure 2.8): This case is also similar to Case 1, with the difference being that the beampattern power has been reduced. As a result, the pulse profile peak is less sharp in the third plot in comparison to Case 1.

Parameter	Case 1	Case 2	Case 3	Case 4	Case 5
Rotational inclination (°)	90	0	90	90	90
Rotational azimuth (°)	0	0	0	0	0
Magnetic colatitude (°)	90	90	0	90	90
Azimuth shift (rad)	0	0	0	0	0
Inclination shift (rad)	0	0	-1.214	0	0
Power (-)	15	15	15	15	1
Relative phase shift (rad)	0	0	0	π	0

Table 2.1: Values of the neutron star parameters for cases 1 to 5 discussed in Section 2.2. The neutron star mass and radius were fixed to the values of 1.4 $M_\odot$ and 12.4 km, respectively, in all cases.

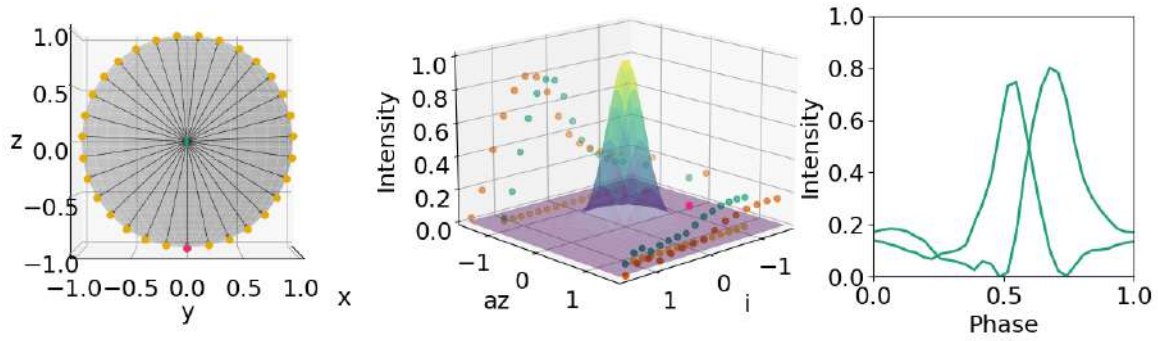

Figure 2.5: Pulse profile plots, as in Figure 2.2, but for Case 2. The parameters are listed in Table 2.1.

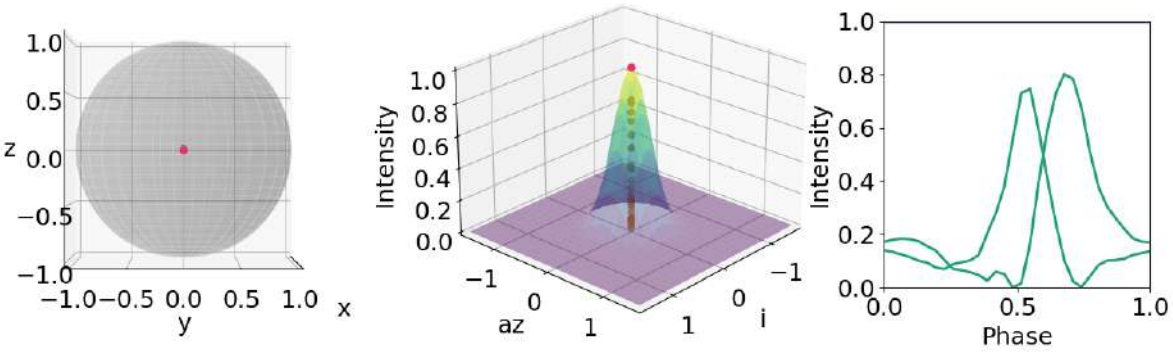

Figure 2.6: Pulse profile plots, as in Figure 2.2, but for Case 3. The parameters are listed in Table 2.1.

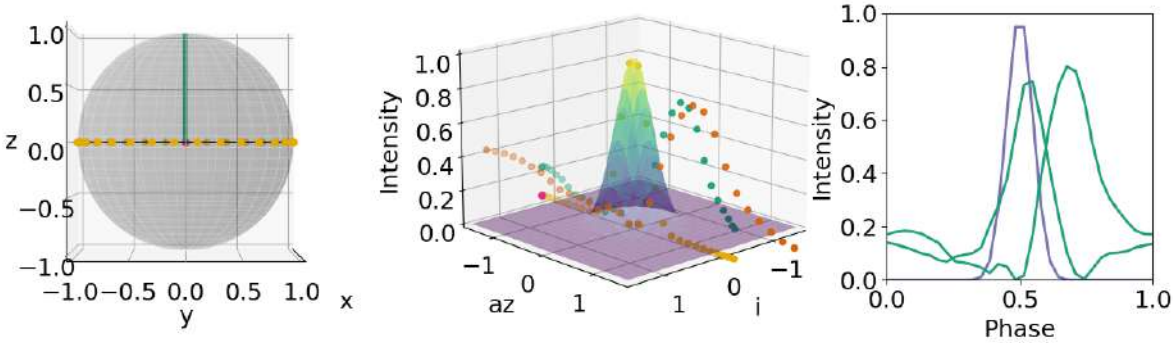

Figure 2.7: Pulse profile plots, as in Figure 2.2, but for Case 4. The parameters are listed in Table 2.1.

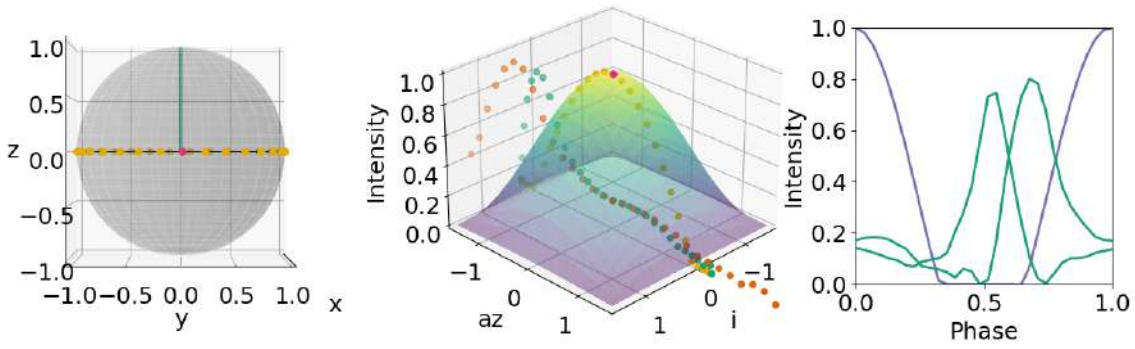

Figure 2.8: Pulse profile plots, as in Figure 2.2, but for Case 5. The parameters are listed in Table 2.1.

2.3 Numerical analysis

To find the most likely properties of the neutron star, that is to say, the parameters that would simulate a pulse profile that would best fit the given data, the particle swarm optimization method was used. The particle swarm method involves having a number of different candidate solutions, called particles, to a particular problem. The problem concerns some measure of quality. Each particle then travels in a search-space of solutions to find the best solution to that problem. In our case, the measure of quality is the minimization of the least square error between the curve we are fitting to the data and each of the pulse profiles. Each particle is in our case one set of values for the neutron star's parameters.

The particle swarm method was applied in two different ways:

1. The simultaneous fitting method: Fit one curve to both given profiles simultaneously;

2. The pole-by-pole fitting method: Fit one curve to each profile with some appropriate conditions. These conditions were that the orientation of the star's rotational axis has to be the same for both poles since they have to be part of the same neutron star. The neutron star's mass and radius are also identical for both poles for the same reason. We applied this method in four different cases where each case had its own additional conditions. These conditions had to do with whether the magnetic colatitude and relative phase shift parameters differ between the poles or not.

In this report, we only focus on the second method. We refer to Appendix A for detailed information about the first method. The second method of optimization was implemented in Python (see Appendix A).

Chapter 3

Properties of Cen X−3

In this Chapter we provide the results of our fit to the pulse profiles adopting the pole-by-pole fitting method presented in Section 2.3. We discuss our results and highlight future avenues.

3.1 Optimization results

For the four cases that depended on the magnetic colatitude and relative phase shift varying between the poles, example results are shown in Figures 3.1, 3.2, and B.1 to B.6. Each figure is a variant of Figure 2.2. The latter six figures are listed in Appendix B due to their overall similarity to the first two plots and for brevity's sake. The parameters and conditions for each case are provided in Tables 3.1 to 3.4. In each table, a green (respectively red) background indicates that the corresponding parameter is allowed (respectively not allowed) to vary between the poles. The cases are as follows:

1. Fit 1: None of the two parameters is allowed to vary between the two poles.
2. Fit 2: Only the relative phase shift is allowed to vary between the two poles.
3. Fit 3: Both parameters are allowed to vary between the two poles.
4. Fit 4: Only the magnetic colatitude is allowed to vary between the two poles.

We here note that the derived parameters are not necessarily the only good parameters. Running the program twice for the same case can give a good fit in both runs albeit with vastly different parameters, see Appendix B.2.

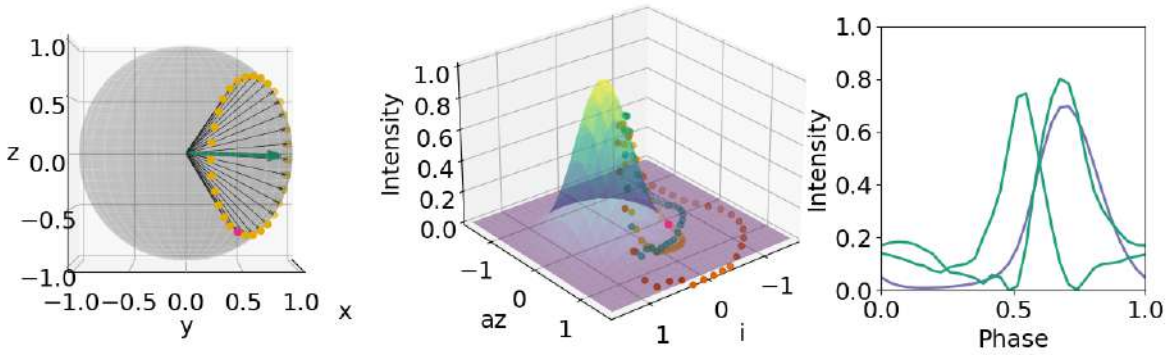

Figure 3.1: Pulse profile plots for Fit 1 (fixed magnetic colatitude and fixed relative phase shift between the two poles). The purple curve on the right plot shows the fit of the right pole. That curve is generated from the parameters visualized in the left and middle plots.

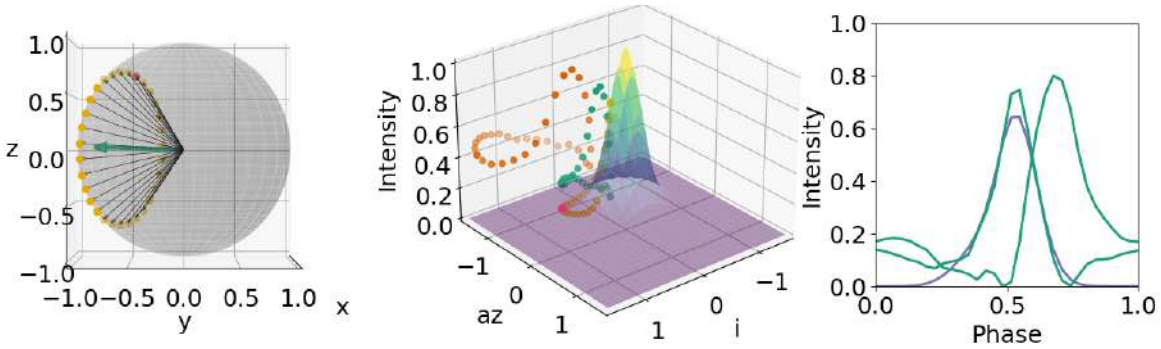

Figure 3.2: Same as Figure 3.1 but for the left pole.

	Right pole	Left pole
Rotational inclination (deg)	-1.44	1.44
Rotational azimuth (deg)	59.28	-120.72
Magnetic colatitude (deg)	46.56	46.56
Azimuth shift (rad)	0.08	0.61
Inclination shift (rad)	-0.38	0.48
Power (-)	7.0	19.87
Neutron star mass ($M_\odot$)	2.56	2.56
Neutron star radius (km)	10.04	10.04
Relative phase shift (rad)	-0.31	3.46

Table 3.1: Values of the neutron star's parameters for Fit 1 (see Figures 3.1 and 3.2).

	Right pole	Left pole
Rotational inclination (deg)	76.32	-76.32
Rotational azimuth (deg)	-135.37	44.63
Magnetic colatitude (deg)	44.48	44.48
Azimuth shift (rad)	2.58	0.05
Inclination shift (rad)	2.16	0.66
Power (-)	4.8	12.88
Neutron star mass ($M_\odot$)	2.36	2.36
Neutron star radius (km)	11.83	11.83
Relative phase shift (rad)	-1.14	0.91

Table 3.2: Values of the neutron star's parameters for Fit 2 (see Figures B.1 and B.2).

	Right pole	Left pole
Rotational Inclination (deg)	38.13	-38.13
Rotational azimuth (deg)	-35.11	144.89
Magnetic colatitude (deg)	55.39	63.43
Azimuth shift (rad)	0.6	-0.47
Inclination shift (rad)	-0.68	3.02
Power (-)	6.0	10.03
Neutron star mass ($M_\odot$)	2.71	2.71
Neutron star radius (km)	11.25	11.25
Relative phase shift (rad)	-0.4	1.13

Table 3.3: Values of the neutron star's parameters for Fit 3 (see Figures B.3 and B.4).

	Right pole	Left pole
Rotational inclination (deg)	-16.13	16.13
Rotational azimuth (deg)	41.61	-138.39
Magnetic colatitude (deg)	53.13	73.41
Azimuth shift (rad)	-0.27	1.97
Inclination shift (rad)	0.83	-0.08
Power (-)	5.21	16.07
Neutron star mass ($M_\odot$)	2.95	2.95
Neutron star radius (km)	11.27	11.27
Relative phase shift (rad)	1.8	1.34

Table 3.4: Values of the neutron star's parameters for Fit 4 (see Figures B.5 and B.6).

Note the relatively high mass values shown in each table.

Finding the most accurate case

After optimizing, we now attempt to find which case is the most accurate to represent reality. To do this, we introduce a metric analogous to the reduced-chi-square method. In this case, we divide the average cost from each case by the corresponding number of degrees of freedom. To get the average cost, we ran five simulations for each case to get five cost values, whereupon we calculated the mean of those values. The cost values are from the fitting of the second pole. The cost value for the fitting of the first pole is ignored due to there being no variation in how the pole is fit. As such, the average cost for this pole will be the same for all four fits and, as a result, it can not be used to find the most accurate fit. This is in contrast to the fitting of the second pole, where different conditions can be imposed upon the fitting, which may allow for differing average costs. The degrees of freedom are obtained by subtracting the number of free parameters from the number of data points. We call the final result the 'cost per parameter'. The lower this value for a given case, the greater the case's potential accuracy. The results are shown in Table 3.5. For the exact fit results obtained for each run of each fit, see Appendix B.2.

	Fits 1	Fits 2	Fits 3	Fits 4
Average cost (-)	0.26	0.12	0.11	0.15
Cost margin of error (-)	±0.21	±0.01	±0.01	±0.02
Degrees of freedom (-)	29	28	27	28
Cost per parameter (-)	0.0091	0.0042	0.0040	0.0052
Cost per parameter margin of error (-)	±0.0071	±0.0002	±0.0005	±0.0007

Table 3.5: Average cost, degrees of freedom, and cost per parameter for each of the cases described in Section 3.1. A confidence level of 95% was used when calculating the margins of error.

3.2 Gravitational light bending

Our observations of the effects of gravitational light bending are illustrated in Figure 3.3. We found that the lower the mass-radius ratio of the neutron star, the closer the intrinsic data and the observational points approach the measured data in the beampattern plot. The higher the mass-radius ratio, the more the intrinsic data and observational points approach the center of the plot. If the mass-radius ratio is high enough, these points disappear and no curve can be generated on the pulse profile plot.

3.3 Discussion

3.3.1 Optimization

From Table 3.5, it appears that allowing both the magnetic colatitude and relative phase shift to vary leads to the best possible results for the fit. In other words, Fit 3 appears to be the most accurate case. This indicates that perhaps the magnetic poles of the star are not necessarily antipodal and may not necessarily have an axis that goes through the center of the star.

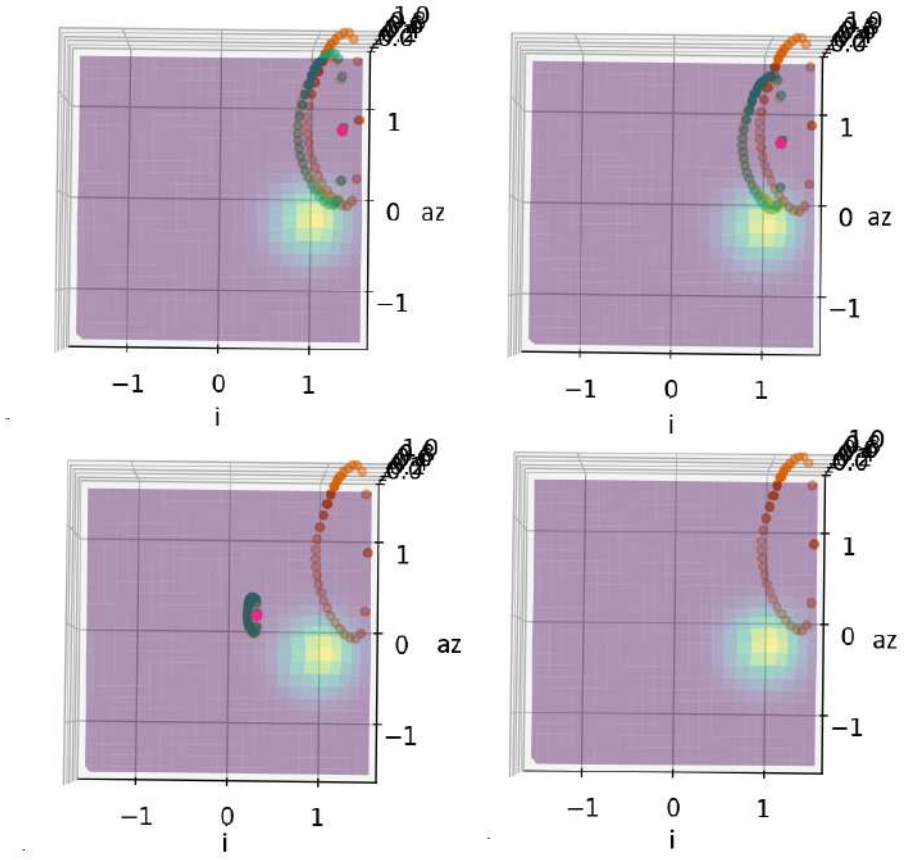

Figure 3.3: Change in the position of the intrinsic data and observation points as the mass-radius ratio is increased. Note how the dots disappear on the fourth plot when the mass-radius ratio is the largest. The approximate mass-radius ratio value in each image is, from left to right and from top to bottom, 0.050, 0.11, 0.33, and 0.34 $M_{\odot}\text{km}^{-1}$.

However, as stated in Section 3.1, the sets of parameters we got as optimization results are not necessarily the only good ones (see Appendix B.2 for more results using the same fit). There is also the fact that the parameter values vary a lot between cases too. If there was only one good set of parameters, then the parameters would have to converge to approximately the same values in all cases, yet it apparently does not. As such, we cannot immediately draw any firm conclusion on the properties of Centaurus X-3. Also, Fit 3 having the lowest cost per parameter value could just be because the program had more free parameters. It could also be because we only ran five simulations for each case when calculating the cost per parameter.

Despite the optimization not converging to a single set of parameters, it is not restrictive in the present project. This is because we are looking for possible solutions to see if our toy model can explain the observations. The fitting of both poles is a much more complex problem and for the final correct solution we need to take into account radiative transfer which is beyond the scope of this work.

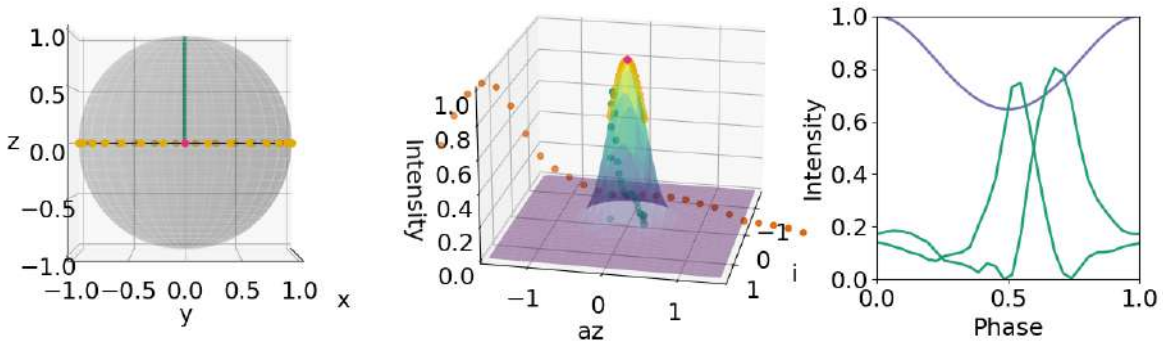

Figure 3.4: Same as Figure 2.4, but the mass-radius ratio is significantly increased. The observation points all approach the center of the middle plot which results in a pulse profile that is always visible regardless of the phase, implying that the light from the emitted beam is being bent in the direction of the Earth.

3.3.2 Gravitational light bending

As was shown in Section 3.2, the measured data are being approached by the other points when the mass-radius ratio is decreased (so that it is lower than around 0.050 $M_{\odot}\text{km}^{-1}$). A low mass-radius ratio means that the neutron star has a relatively low density (which in this case is around 2.38×10^{19} kg m^{-3} at most). So the lower the star density is, the less discrepancy there is between the measured and intrinsic data points. This suggests that gravitational light bending becomes weaker for decreasing density which is consistent with what we expect.

The intrinsic data and observation points all approaching the center of the plot and each other as the mass-radius ratio or density is increased is expected since the light bending becomes so strong that if the beampattern happens to be on one of those observation points, it will always be observable from the Earth regardless of the neutron star's orientation. This implies that a large portion of the light emitted from the neutron star is bent by gravity in the direction of the Earth. For an illustrative example, see Figure 3.4.

Those points disappearing when the mass-radius ratio or density is higher (when the mass-radius ratio is around 0.34 $M_{\odot}\text{km}^{-1}$, corresponding to a density of around 1.61×10^{20} kg m^{-3}) implies that the density has reached a point where Equation (1.1) no longer applies. If the term r_g/R, which is proportional to the mass-radius ratio, becomes too large, $\cos(\alpha)$ goes outside the range of [-1, 1] and Equation (1.1) becomes invalid. As such, the points disappearing on the plot is a reflection of Equation (1.1) becoming invalid. However, we have already found good fits using Equation (1.1) and we have to consider that the average neutron star density is far lower than the calculated density required for gravitational light bending to have a major effect. For these two reasons, this limitation does not seem to pose any problem in the present context.

3.3.3 Ethical and societal implications

Ethical and societal implications of our project are inexistent.

3.3.4 Future prospects

There are many ways in which this research can be extended and improved.

First, regarding optimization and the pole-by-pole fitting method, more cases of the beam pattern can be studied. In particular, it would be of great interest to investigate the case where the beampattern is fixed for both poles but the position of the axis of symmetry is changing, and see if we can find a more accurate result than those we found.

Second, there is a simpler least-square optimization method that we may want to consider. It involves only one set of values for the neutron star's parameters which would serve as the initial values before optimization. This set of values would then be slightly shifted to higher or lower values, after which the least square error between the curves would be calculated. This method is perhaps easier to understand conceptually than the particle swarm method, but the latter proved to be computationally superior on top of having a wider reach when searching for solutions, so we chose to work with that one in the present project.

Third, it is relevant to mention that we did not use the standard spherical coordinates in our research, but a variation of it instead. If we want to perform analytical calculations, it would be better to convert the coordinates to the standard spherical coordinate system.

Fourth, the beampattern plot can be simplified visually by converting it into a contour line plot without loss of information.

Aside from Equation (1.1), we used a few other assumptions and simplifications. Notably, we assumed that the beampatterns azimuth and inclination shift are the only sources of asymmetry and that the beam intensity is distributed like a 2D-cosine plot. It would be of great interest to investigate cases where these assumptions are removed.

Chapter 4

Summary and conclusions

We analyzed the pulse profiles of Centaurus X−3 using a toy model to derive potential parameters for the neutron star. We varied several parameters in the toy model to achieve this goal. These include the rotation axis orientation, the magnetic axis orientation, the beampattern location and power, the neutron star mass and radius, and the rotational relative phase shift. Our method involved fitting the two pulse profiles one after the other.

We established a few conditions on the parameters to ensure the final fit is in line with reality. We fitted for four different cases, each with their own additional conditions, using the particle swarm method to find the best-fitting parameters. These cases depend on whether the magnetic colatitude and relative phase shift were allowed to vary between the two poles. We obtained good fits in each case, so we went on to try and find the one that was probably the most accurate. It appeared that the best case is obtained if both the magnetic colatitude and relative phase shift are allowed to vary, though that is not necessarily a good conclusion since one can get several different good parameter fits for each simulation and also because this case had more free parameters than the other cases. Future investigations involving the inclusion of radiative transfer in the code are required to be able to isolate the most likely set of parameters from the others.

Another aspect we studied was the effect of gravitational light bending on the pulse profiles. In order to do this, we had the neutron star's mass and radius as values we could vary. We used Equation (1.1) which holds for stars with relatively low densities (densities up to around 2.4×10^{19} kg m^{-3}). Our conclusion was that the higher the density of the star, the more important the impact of gravity on light. This causes us to be able to observe the beampattern from Earth even if it is not directly facing us. On the one hand, if the density was high enough (around 1.6×10^{20} kg m^{-3}), the approximation we used no longer applied. This is supported by the relevant data points in our program vanishing. On the other hand, if the density was really low, gravity seemed to have a reduced effect on light, as expected.

The assumptions and simplifications we used can be potential limitations, and future investigations may look into alleviating these restrictions. These include the exclusion of beampattern asymmetry and the assumption that the beampattern is a simple 2D cosine.

There are ways in which our research can be extended. This includes optimization when assuming the poles are antipodal, converting the modified spherical coordinates we used to the standard spherical coordinates, and replacing the 3D beampattern plot by a 2D contour line plot for visualization's sake.

Overall, we have established a good basis on which further research can be built to achieve more conclusive results.

Appendix A: Optimization codes

A.1. Pole-by-pole fitting method

For the second method described in Section 2.3, the following code was implemented when fitting for the first pole:

```
def optimization1(x, y_true):

    """
    Optimization function that fits a curve onto the two profiles by minimizing the least square difference between the curve and each profile.

    Parameters:
    - Particles (Nested list): A nested list where each element is a particle in the swarm, and where each particle has their own parameters to update the fitting curve with
    - Pulse profiles (Nested list): A nested list containing two elements where each element is the data for one pulse profile.

    Returns:
    - An array containing the calculated least square error for each particle in the swarm.
    """

    msev = []
    for i in range(len(x)):
        y_pred = update_least_square(x[i][0], x[i][1], x[i][2],
                                     x[i][3], x[i][4], x[i][5],
                                     x[i][6], x[i][7], x[i][8])

        # Calculate the squared differences and sum them up
        squared_diff_sum0 = sum((y_true[0][i] - y_pred[i]) ** 2 for i in range(len(y_true[0])))
        #squared_diff_sum1 = sum((y_true[1][i] - y_pred[i]) ** 2 for i in range(len(y_true[1])))

        # Calculate the mean squared error
        mse0 = squared_diff_sum0 / len(y_true)
        #mse1 = squared_diff_sum1 / len(y_true)


        msev.append(mse0)

    return msev

optimiser = ps.single.GlobalBestPSO(n_particles=100,
```

```
                                    dimensions=9,
                                    options={'c1': 0.2, 'c2': 0.2,
                                             'w': 0.8},
                                    bounds=(
np.array([-90, -180, 0, -np.pi, -np.pi, 1, 0.8, 8, -np.pi]),
np.array([90, 180, 90, np.pi, np.pi, 20, 3, 13, np.pi])))

k0, k1 = optimiser.optimize(optimization1, 50,
y_true=[decompositions()[0], decompositions()[1]])

update_least_square(
k1[0], k1[1], k1[2], k1[3], k1[4], k1[5], k1[6], k1[7], k1[8])
update_geometry_least_square
k1[0], k1[1], k1[2], k1[3], k1[4], k1[5], k1[6], k1[7], k1[8])
update_beampattern_least_square(
k1[0], k1[1], k1[2], k1[3], k1[4], k1[5], k1[6], k1[7], k1[8])
```

Listing 1: One-by-one profile optimization for the first pole.

The three update functions at the bottom serve to update each plot after the best possible fitting parameters have been found.

For the second pole, a modified version of the code above was used. A second function, called `optimization2` was created. It is similar in structure to the first one with the main difference being the conditions described previously. Hereafter is the code that describes `optimization2` in the example case where the magnetic colatitude and relative phase shift are the same for both poles:

```
def change_ra(a):
    """
    Function that flips rotation azimuth 180 degrees to ensure this
    pole's end of the rotational axis is on the opposite side of the
    other axis end.

    Parameters:
    - Rotational azimuth for the first pole in degrees (variable)

    Returns:
    - Rotational azimuth for the other pole in degrees(variable)
    """
    a += 180
    if a > 180:
        a -= 360
    return a


def change_rps(r):
    """
    Function that calculates relative phase shift for second pole to
    ensure that there is no phase difference between the poles.

    Parameters:
    - Relative phase shift for first pole in radians (variable)

    Returns:
    - Relative phase shift for second pole in radians (variable)
    """
    r += np.pi-2*r
```

```
    return r

def optimization2(x, y_true):

    msev = []
    for i in range(len(x)):
        y_pred = update_least_square2(-k1[0], change_ra(k1[1]), k1[2],
                                      x[i][0], x[i][1], x[i][2], k1[6],
                                      k1[7], change_rps(k1[8]))

        # Calculate the squared differences and sum them up
        #squared_diff_sum0 = sum((y_true[0][i] - y_pred[i]) ** 2 for i
         in range(len(y_true[0])))
        squared_diff_sum1 = sum((y_true[1][i] - y_pred[i]) ** 2 for i
        in range(len(y_true[1])))

        # Calculate the mean squared error
        #mse0 = squared_diff_sum0 / len(y_true)
        mse1 = squared_diff_sum1 / len(y_true)


        msev.append(mse1)

    return msev

optimiser = ps.single.GlobalBestPSO(n_particles=100,
                                    dimensions=3,
                                    options={'c1': 0.2, 'c2': 0.2,
                                             'w': 0.8},
                                    bounds=(
                                    np.array([-np.pi, -np.pi, 1]),
                                    np.array([np.pi, np.pi, 20])))
l0, l1 = optimiser.optimize(optimization2, 50,
y_true=[decompositions()[0], decompositions()[1]])

update_least_square2(
-k1[0], chage_ra(k1[1]), k1[2], l1[0], l1[1], l1[2], k1[6], k1[7],
    change_rps(k1[8])
update_geometry_least_square(
-k1[0], change_ra(k1[1]), k1[2], l1[0], l1[1], l1[2], k1[6], k1[7],
    change_rps(k1[8])
update_beampattern_least_square(
-k1[0], change_ra(k1[1]), k1[2], l1[0], l1[1], l1[2], k1[6], k1[7],
    change_rps(k1[8])
```

Listing 2: One-by-one profile optimization for the second pole.

A.2. Simultaneous fitting method

As stated in Section 2.3, another avenue for finding a good fit to the observations is to fit one curve simultaneously to both pulse profiles. The fit is simultaneous in the sense that the curve is being fit to minimize the sum of the least square errors between the curve and each profile. While we chose to focus on the pole-by-pole fitting method, this other method should not be overlooked, since a good fit would imply that the poles have similar parameter values and would support the idea that the neutron star has uniform

properties.

For this method, the following code was used:

```
def optimization(x, y_true):

    """
    Optimization function that fits a curve onto the two profiles by minimizing the least square difference between the curve and each profile.

    Parameters:
    - Particles (Nested list): A nested list where each element is a particle in the swarm, and where each particle has their own parameters to update the fitting curve with
    - Pulse profiles (Nested list): A nested list containing two elements where each element is the data for one pulse profile.

    Returns:
    - An array containing the calculated least square error for each particle in the swarm.
    """

    msev = []
    for i in range(len(x)):
        y_pred = update_least_square(x[i][0], x[i][1], x[i][2],
                                     x[i][3], x[i][4], x[i][5],
                                     x[i][6], x[i][7], x[i][8])

        # Calculate the squared differences and sum them up
        squared_diff_sum0 = sum((y_true[0][i] - y_pred[i]) ** 2 for i in range(len(y_true[0])))
        squared_diff_sum1 = sum((y_true[1][i] - y_pred[i]) ** 2 for i in range(len(y_true[1])))

        # Calculate the mean squared error
        mse0 = squared_diff_sum0 / len(y_true)
        mse1 = squared_diff_sum1 / len(y_true)


        msev.append(mse0+mse1)

    return msev

optimiser = ps.single.GlobalBestPSO(n_particles=100,
                                    dimensions=9,
                                    options={'c1': 0.2, 'c2': 0.2,
                                             'w': 0.8},
                                    bounds=(
np.array([-90, -180, 0, -np.pi, -np.pi, 1, 0.8, 8, -np.pi]),
np.array([90, 180, 90, np.pi, np.pi, 20, 3, 13, np.pi])))

k0, k1 = optimiser.optimize(optimization1, 50,
y_true=[decompositions()[0], decompositions()[1]])

update_least_square(
k1[0], k1[1], k1[2], k1[3], k1[4], k1[5], k1[6], k1[7], k1[8])
update_geometry_least_square
```

```
k1[0], k1[1], k1[2], k1[3], k1[4], k1[5], k1[6], k1[7], k1[8])
update_beampattern_least_square(
k1[0], k1[1], k1[2], k1[3], k1[4], k1[5], k1[6], k1[7], k1[8])
```

Listing 3: Simultaneous profile optimization.

Appendix B: Additional figures and tables

B.1. Additional figures for the original optimization

This section contains the results obtained for fits 2, 3, and 4 during the original attempt to optimize curves for the pulse profiles (see Section 3.1).

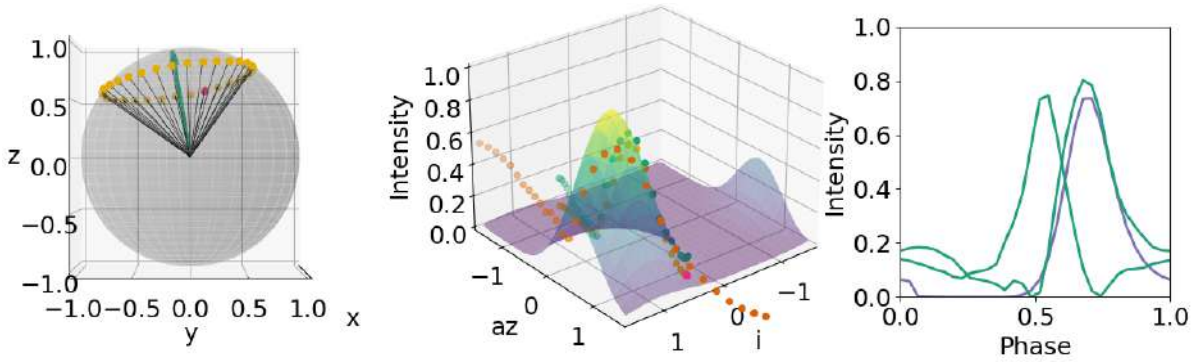

Figure B.1: Same as Figure 3.1 but for fit 2 and right pole.

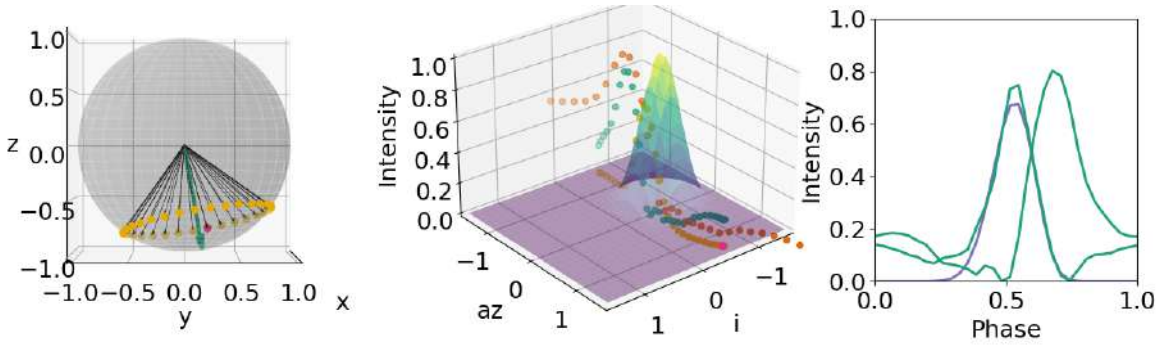

Figure B.2: Same as Figure 3.1 but for fit 2 and left pole.

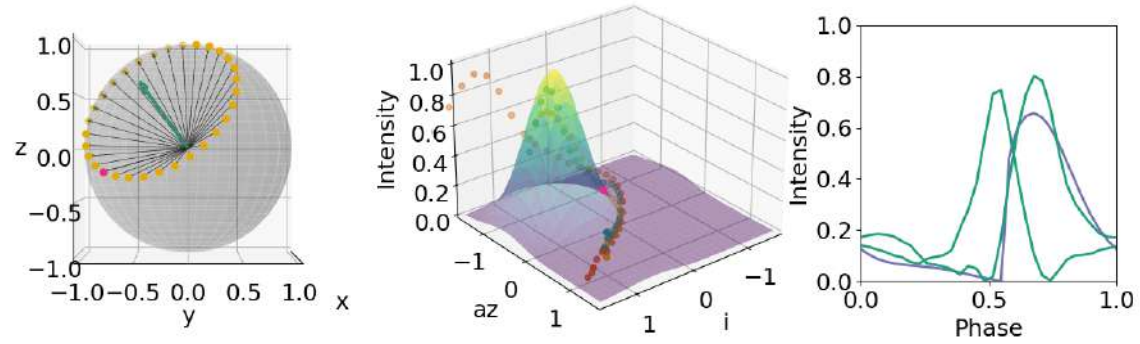

Figure B.3: Same as Figure 3.1 but for fit 3 and right pole.

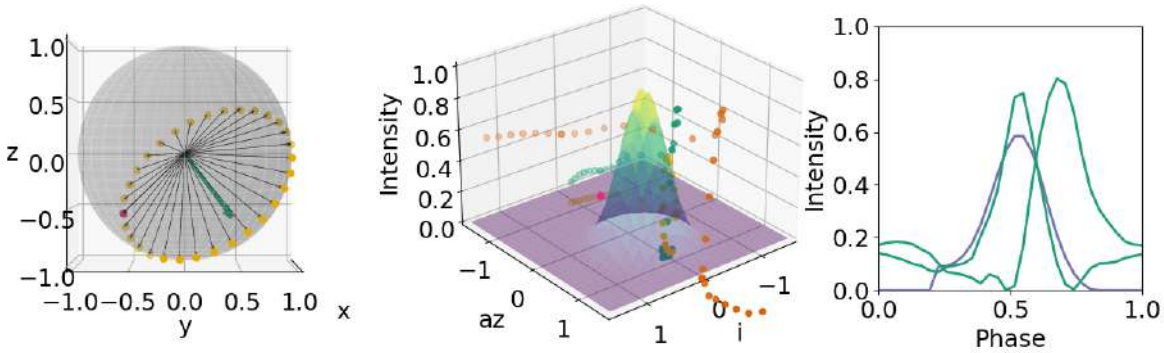

Figure B.4: Same as Figure 3.1 but for fit 3 and left pole.

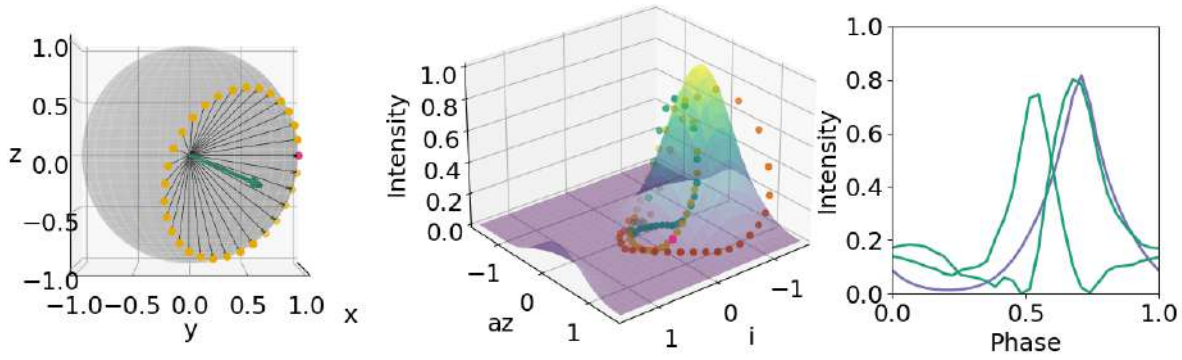

Figure B.5: Same as Figure 3.1 but for fit 4 and right pole.

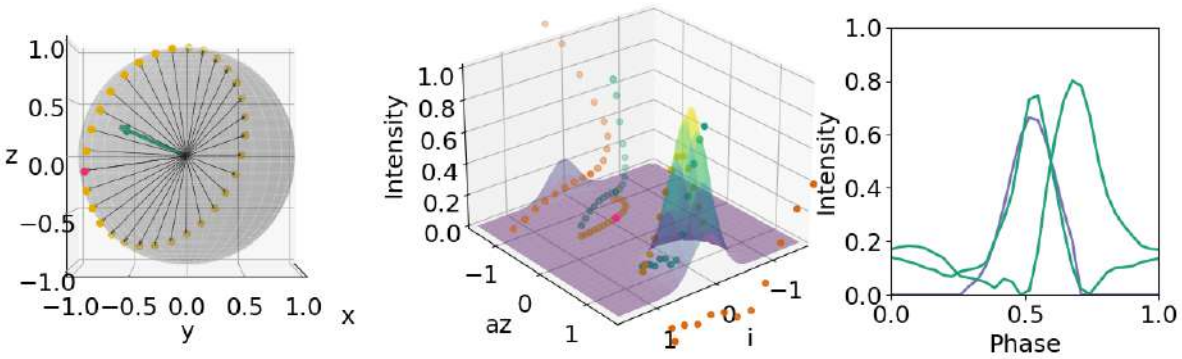

Figure B.6: Same as Figure 3.1 but for fit 4 and left pole.

B.2. Additional figures and tables for the calculation of the cost per parameter

This section contains the results obtained for all fits when calculating the cost per parameter for each fit. Note the on average high mass values shown in each table.

B.2.1. Fit 1

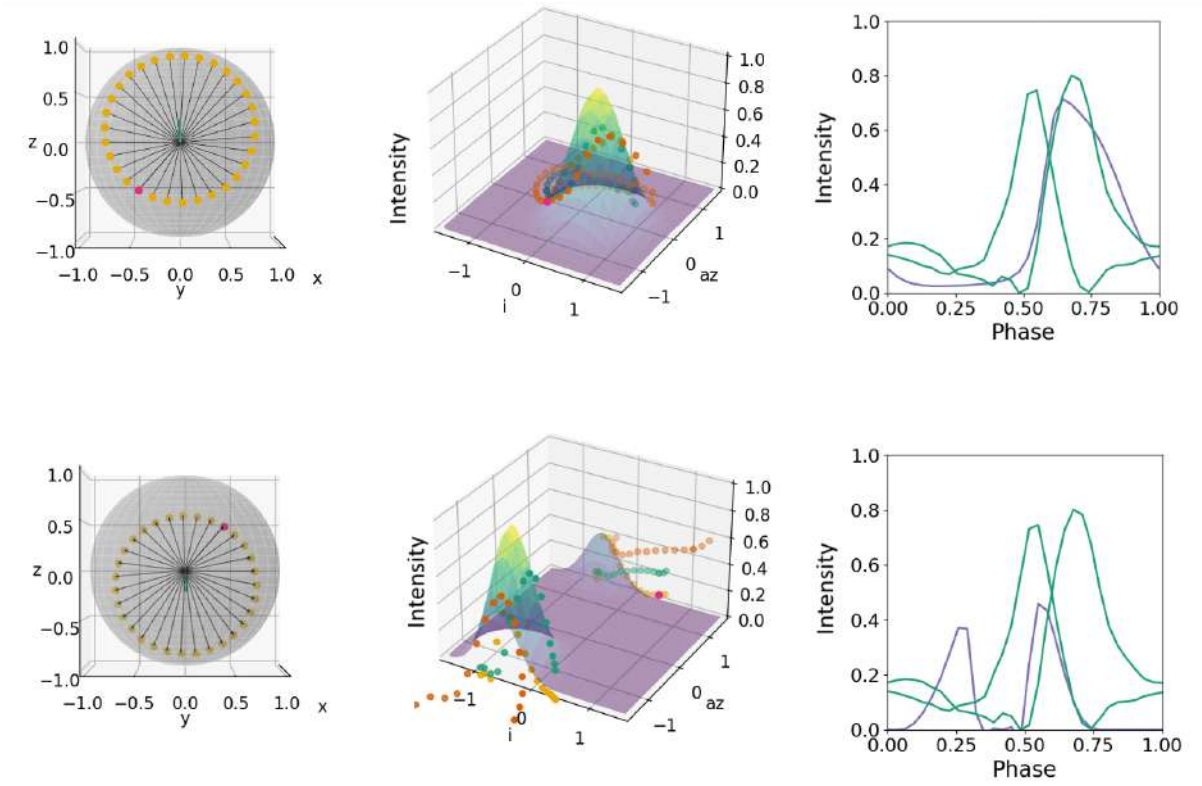

Figure B.7: Same as Figure 3.1 but for the first result for Fit 1, right pole (upper panels) and left pole (lower panels). The parameters are listed in Table B.1.

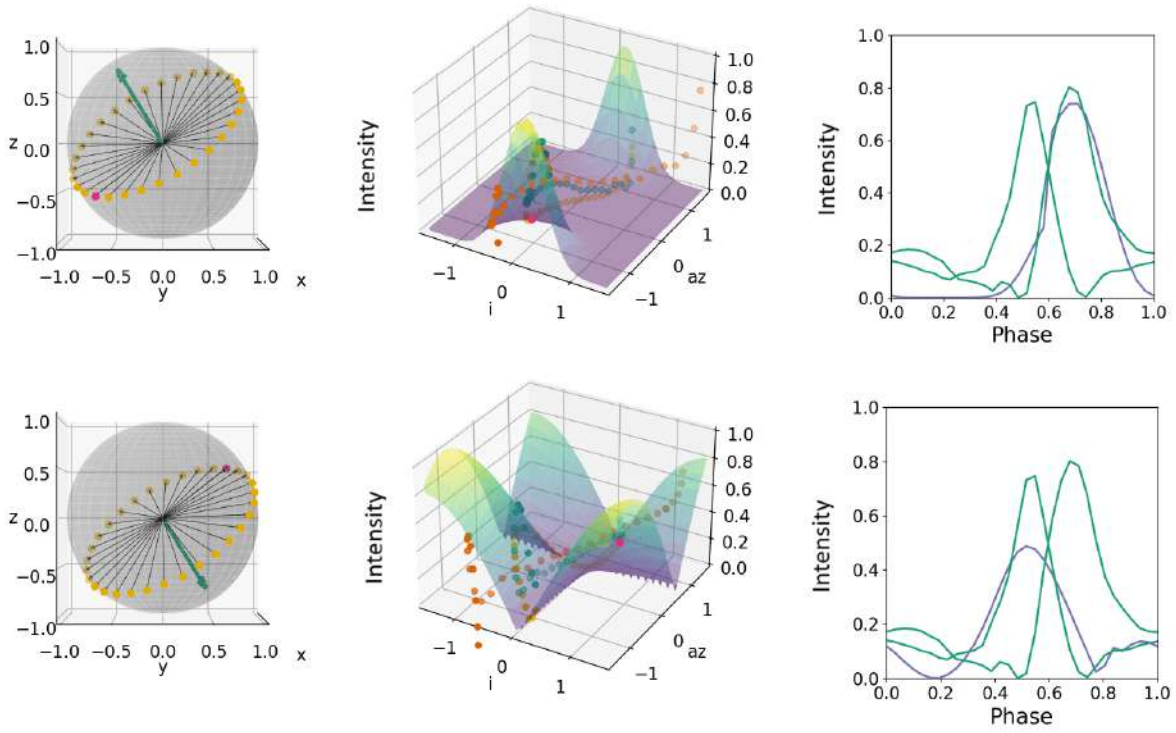

Figure B.8: Same as Figure 3.1 but for the second result for Fit 1, right pole (upper panels) and left pole (lower panels). The parameters are listed in Table B.1.

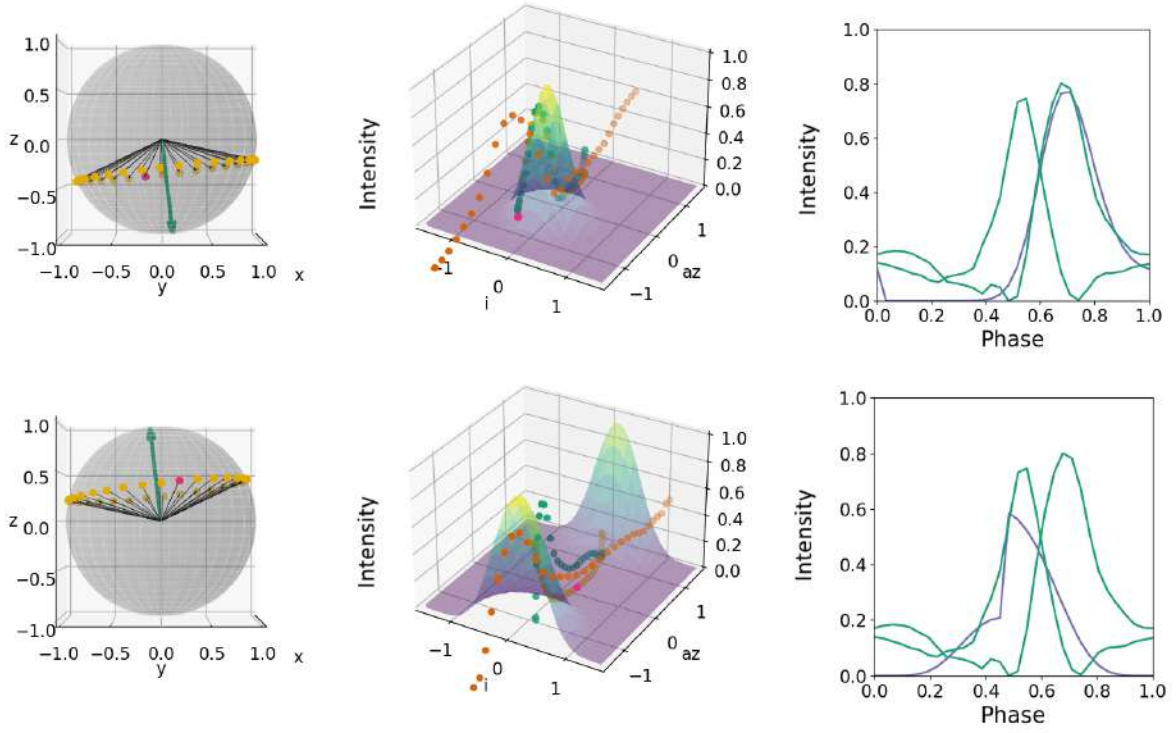

Figure B.9: Same as Figure 3.1 but for the third result for Fit 1, right pole (upper panels) and left pole (lower panels). The parameters are listed in Table B.1.

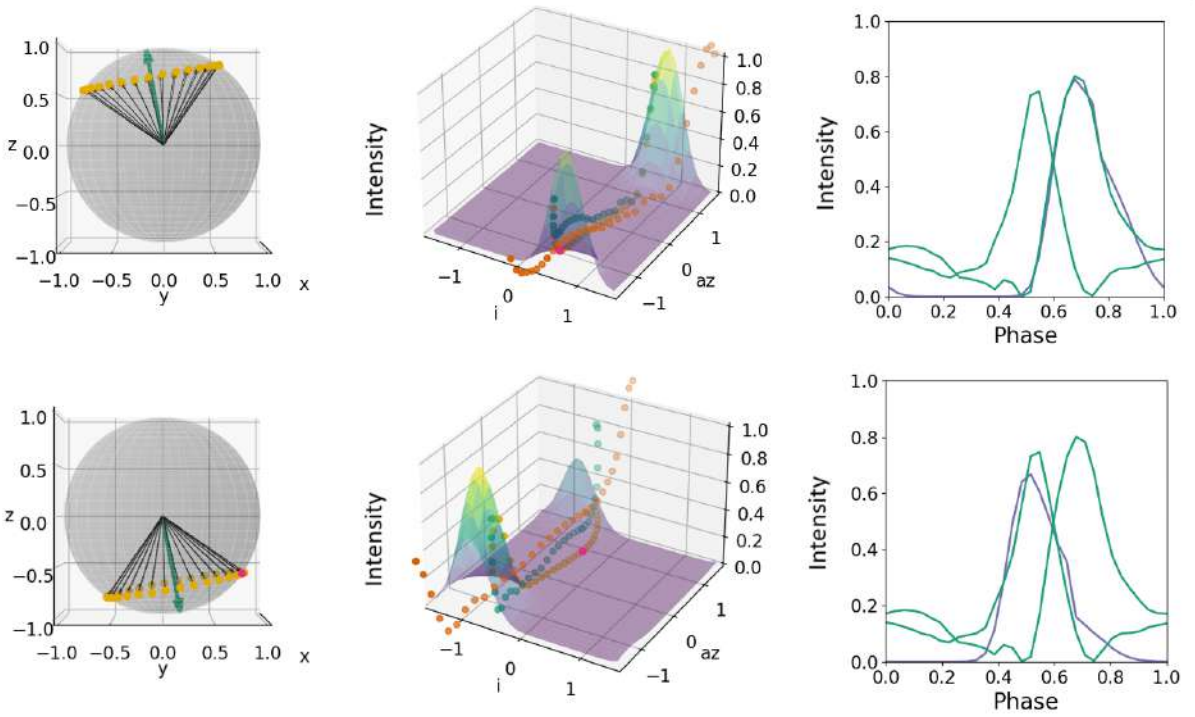

Figure B.10: Same as Figure 3.1 but for the fourth result for Fit 1, right pole (upper panels) and left pole (lower panels). The parameters are listed in Table B.1.

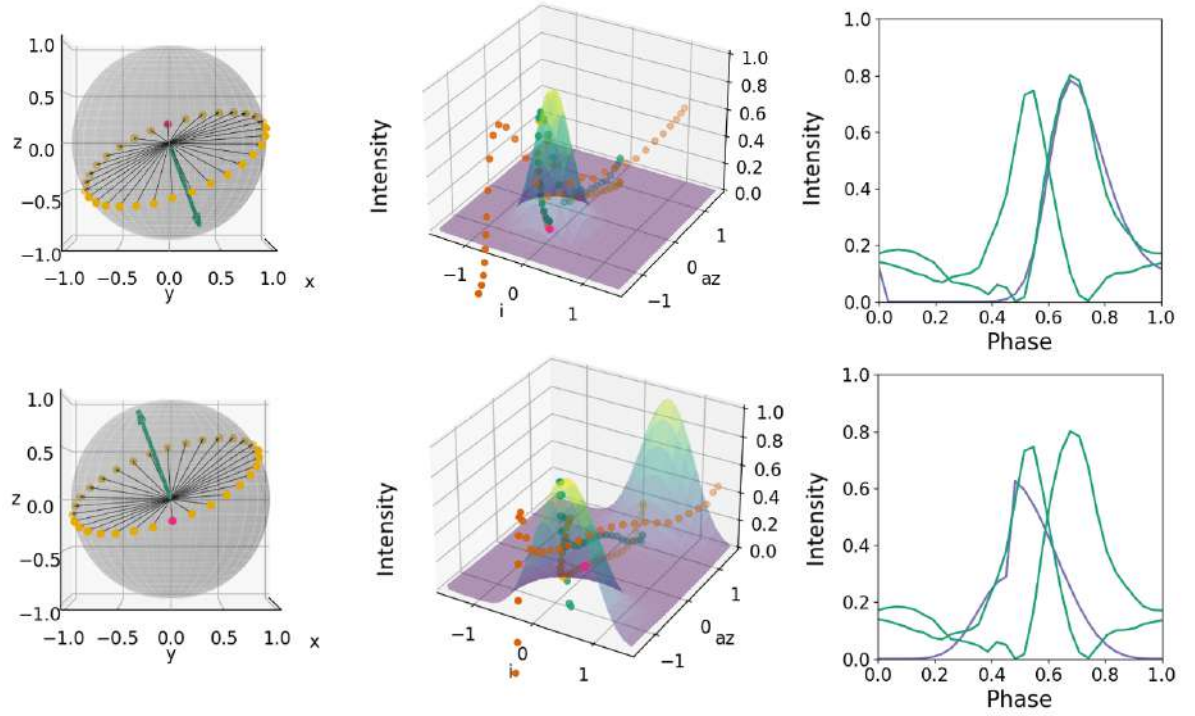

Figure B.11: Same as Figure 3.1 but for the fifth result for Fit 1, right pole (upper panels) and left pole (lower panels). The parameters are listed in Table B.1.

	Result 1	Result 2	Result 3	Result 4	Result 5
	Right pole	Right pole	Right pole	Right pole	Right pole
Rotational inclination (deg)	13.15	48.84	-82.49	79.5	-60.78
Rotational azimuth (deg)	-0.5	-44.78	63.3	-84.42	138.66
Magnetic colatitude (deg)	49.84	81.3	70.79	45.2	79.89
Azimuth shift (rad)	0.27	-1.7	0.47	1.67	0.55
Inclination shift (rad)	-0.45	3.0	-0.01	2.37	0.13
Power (-)	6.02	8.9	12.19	15.14	14.98
Neutron star mass ($M_\odot$)	1.67	2.41	2.44	2.35	2.9
Neutron star radius (km)	11.93	10.73	9.45	12.79	11.38
Relative phase shift (rad)	-0.57	-0.13	0.86	-0.39	2.41
	Left pole	Left pole	Left pole	Left pole	Left pole
Rotational inclination (deg)	-13.15	-48.84	82.49	-79.5	60.78
Rotational azimuth (deg)	179.5	135.22	-116.7	95.58	-41.34
Magnetic colatitude (deg)	49.84	81.3	70.79	45.2	79.89
Azimuth shift (rad)	1.16	0.95	-1.71	1.25	1.44
Inclination shift (rad)	0.6	-1.63	-0.11	0.88	-0.44
Power (-)	10.11	1.51	6.4	12.31	5.15
Neutron star mass ($M_\odot$)	1.67	2.41	2.44	2.35	2.9
Neutron star radius (km)	11.93	10.73	9.45	12.79	11.38
Relative phase shift (rad)	3.71	3.27	2.28	3.54	0.73

Table B.1: Table showing all the results obtained when calculating the cost per parameter for Fit 1.

	Result 1	Result 2	Result 3	Result 4	Result 5
Cost	0.68	0.14	0.18	0.15	0.16

Table B.2: The cost obtained for each result when calculating the cost per parameter for Fit 1.

B.2.2. Fit 2

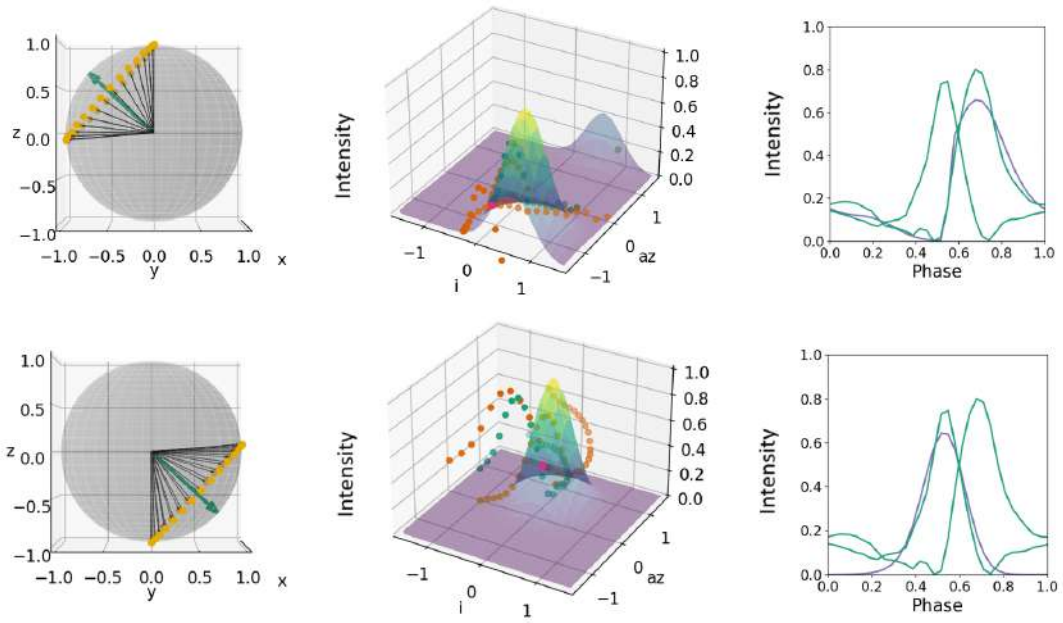

Figure B.12: Same as Figure 3.1 but for the first result for Fit 2, right pole (upper panels) and left pole (lower panels). The parameters are listed in Table B.3.

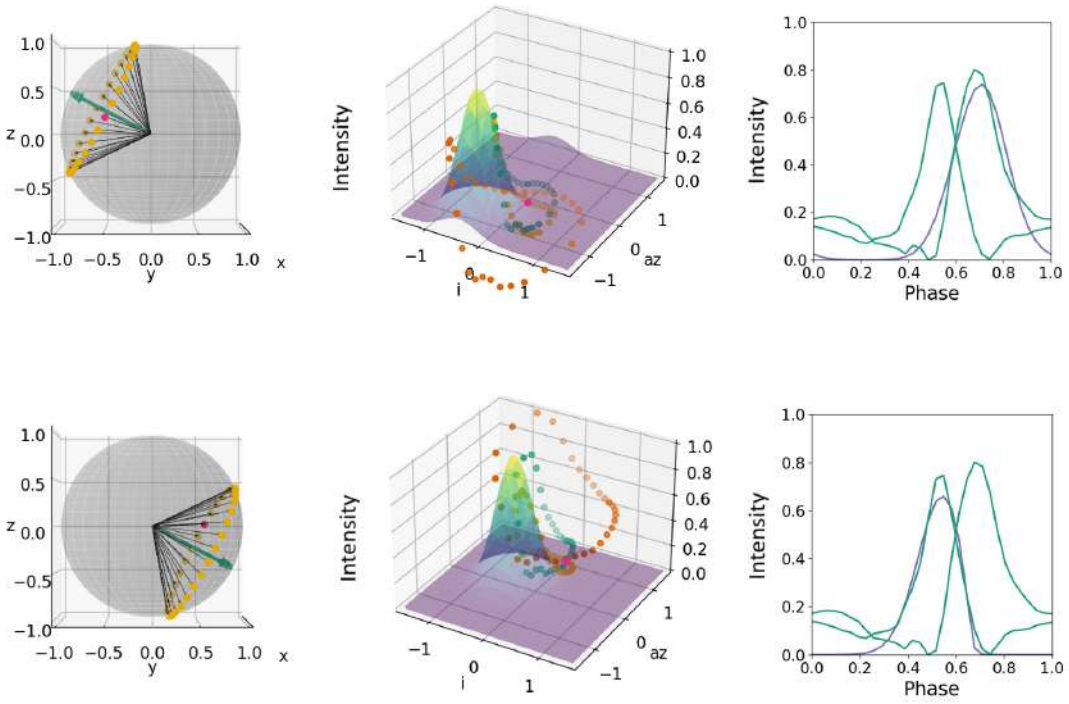

Figure B.13: Same as Figure 3.1 but for the second result for Fit 2, right pole (upper panels) and left pole (lower panels). The parameters are listed in Table B.3.

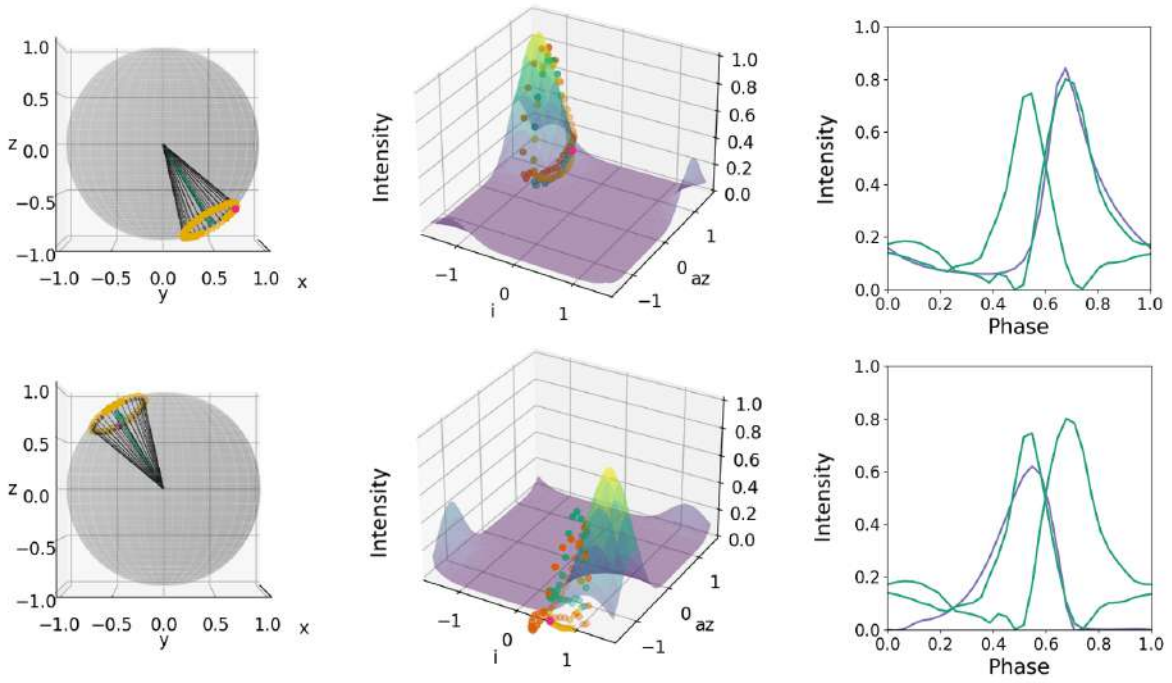

Figure B.14: Same as Figure 3.1 but for the third result for Fit 2, right pole (upper panels) and left pole (lower panels). The parameters are listed in Table B.3.

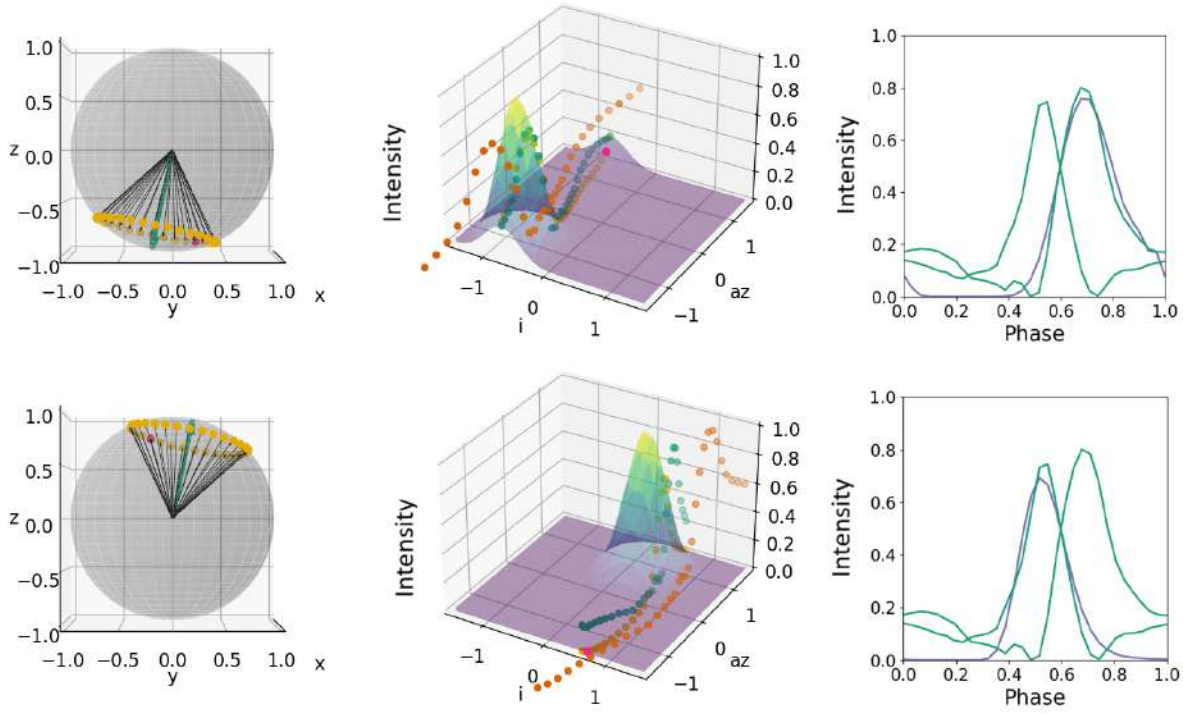

Figure B.15: Same as Figure 3.1 but for the fourth result for Fit 2, right pole (upper panels) and left pole (lower panels). The parameters are listed in Table B.3.

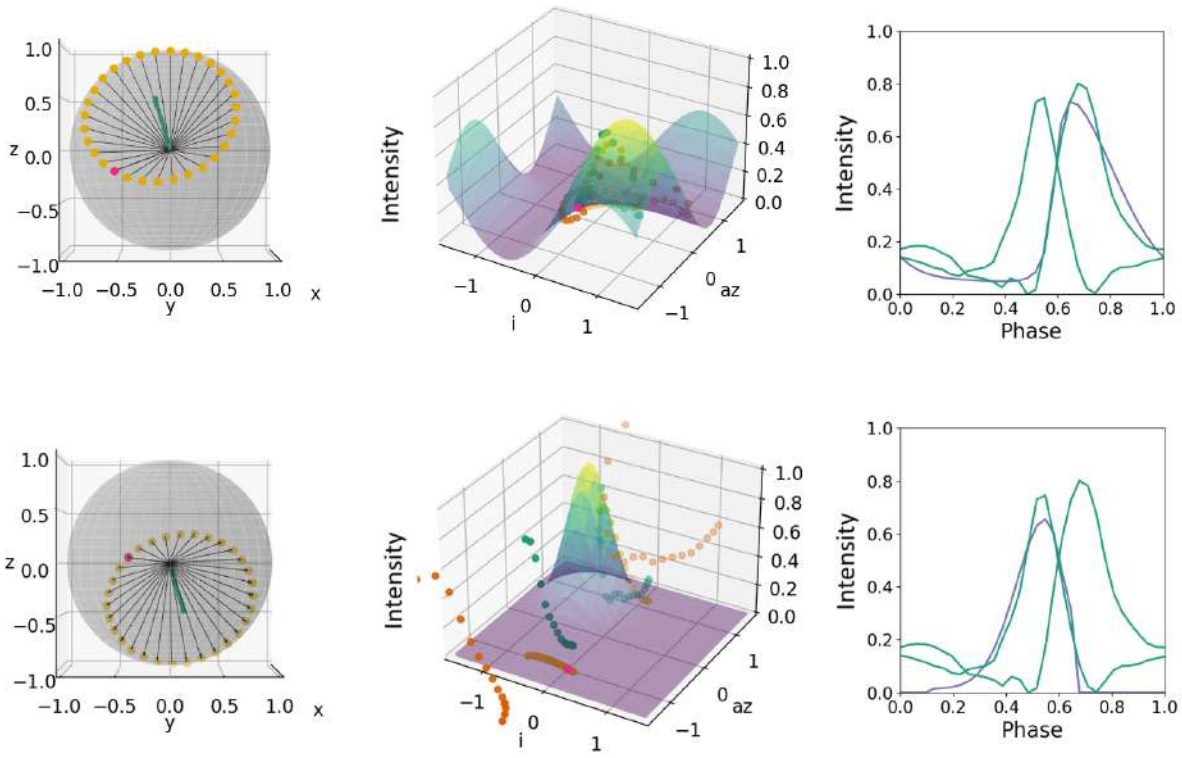

Figure B.16: Same as Figure 3.1 but for the fifth result for Fit 2, right pole (upper panels) and left pole (lower panels). The parameters are listed in Table B.3.

	Result 1	Result 2	Result 3	Result 4	Result 5
	Right pole	Right pole	Right pole	Right pole	Right pole
Rotational inclination (deg)	42.72	27.06	-54.82	-76.35	30.47
Rotational azimuth (deg)	-91.06	-82.68	60.15	-57.58	-9.84
Magnetic colatitude (deg)	47.44	52.46	18.21	36.53	47.52
Azimuth shift (rad)	1.12	-2.21	-0.99	1.08	-2.27
Inclination shift (rad)	-0.61	0.41	1.15	0.73	-1.0
Power (-)	8.51	10.97	10.01	13.6	2.66
Neutron star mass ($M_\odot$)	2.22	2.69	1.22	1.81	2.74
Neutron star radius (km)	11.78	10.73	9.57	10.5	10.93
Relative phase shift (rad)	-0.19	1.44	2.27	-0.27	-0.55
	Left pole	Left pole	Left pole	Left pole	Left pole
Rotational inclination (deg)	-42.72	-27.06	54.82	76.35	-30.47
Rotational azimuth (deg)	88.94	97.32	-119.85	122.42	170.16
Magnetic colatitude (deg)	47.44	52.46	18.21	36.53	47.52
Azimuth shift (rad)	2.75	-0.03	-2.14	2.45	2.54
Inclination shift (rad)	-0.14	0.41	-1.16	-0.33	0.59
Power (-)	9.11	11.15	9.38	11.07	10.33
Neutron star mass ($M_\odot$)	2.22	2.69	1.22	1.81	2.74
Neutron star radius (km)	11.78	10.73	9.57	10.5	10.93
Relative phase shift (rad)	0.77	2.01	-0.96	1.7	2.25

Table B.3: Table showing all the results obtained when calculating the cost per parameter for Fit 2.

	Result 1	Result 2	Result 3	Result 4	Result 5
Cost	0.12	0.11	0.12	0.13	0.11

Table B.4: The cost obtained for each result when calculating the cost per parameter for Fit 2.

B.2.3. Fit 3

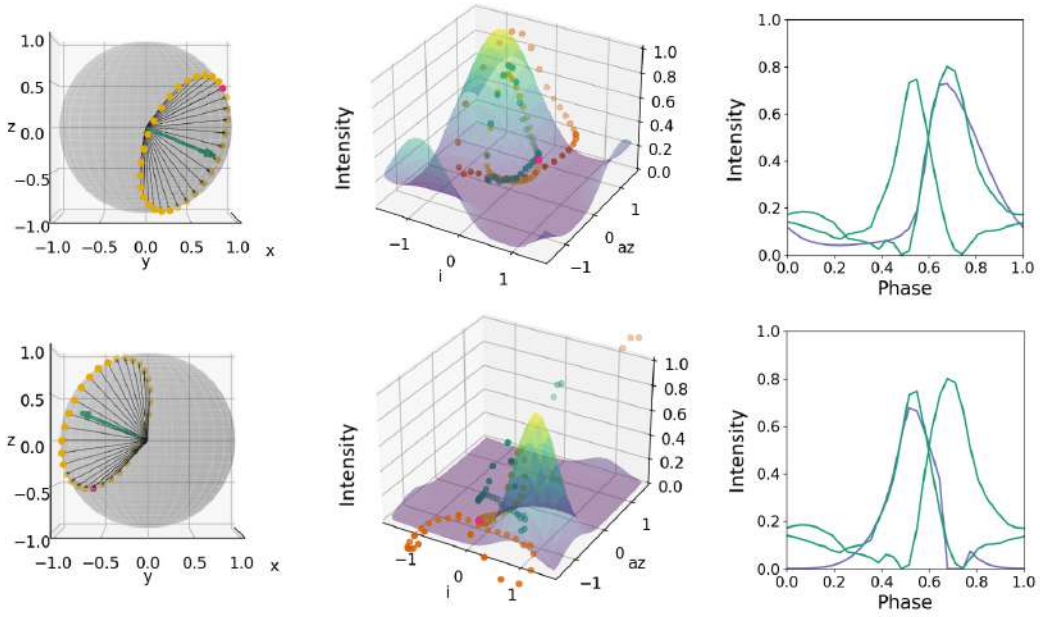

Figure B.17: Same as Figure 3.1 but for the first result for Fit 3, right pole (upper panels) and left pole (lower panels). The parameters are listed in Table B.5.

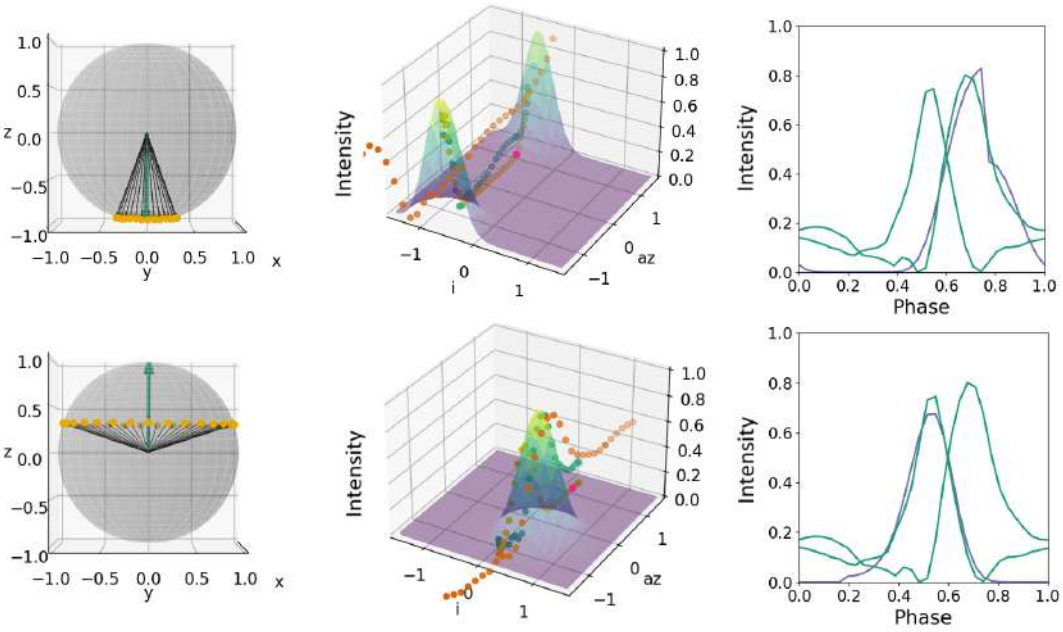

Figure B.18: Same as Figure 3.1 but for the second result for Fit 3, right pole (upper panels) and left pole (lower panels). The parameters are listed in Table B.5.

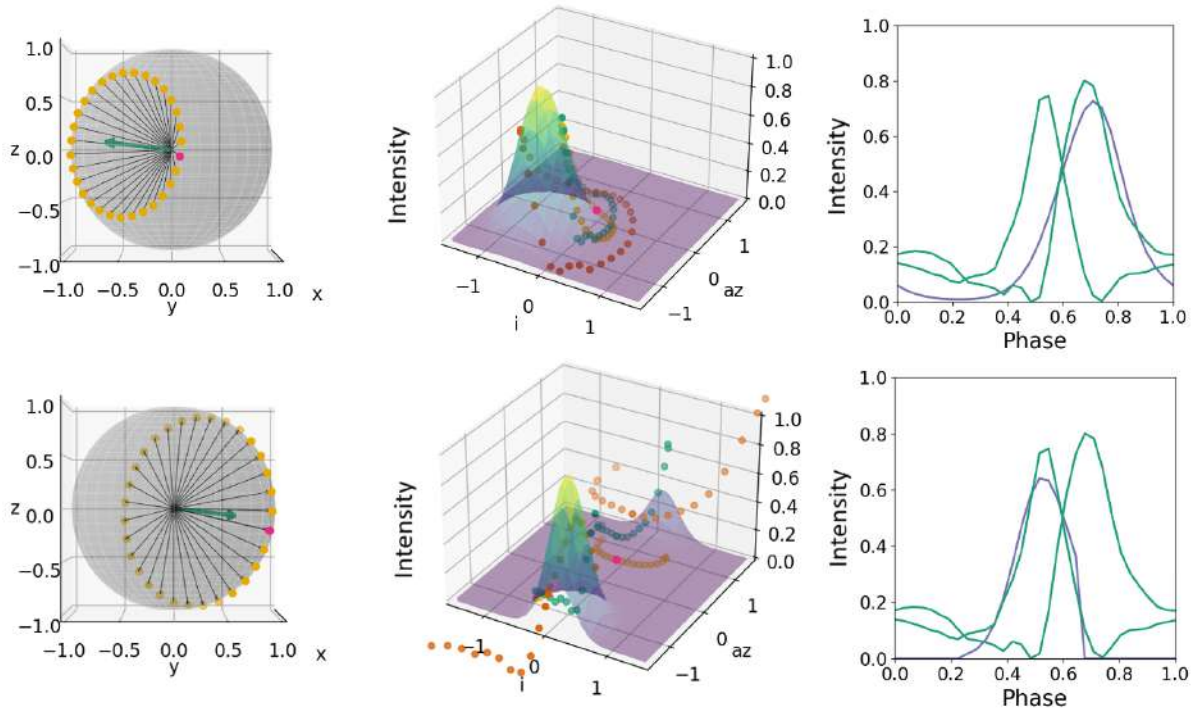

Figure B.19: Same as Figure 3.1 but for the third result for Fit 3, right pole (upper panels) and left pole (lower panels). The parameters are listed in Table B.5.

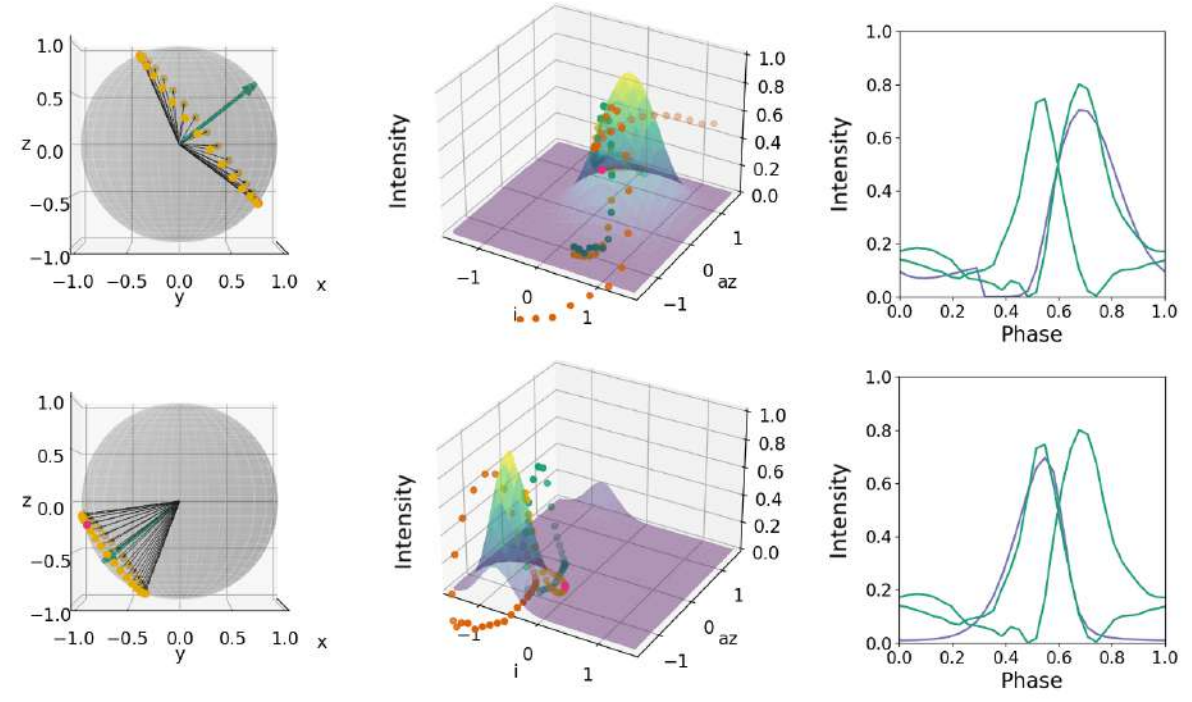

Figure B.20: Same as Figure 3.1 but for the fourth result for Fit 3, right pole (upper panels) and left pole (lower panels). The parameters are listed in Table B.5.

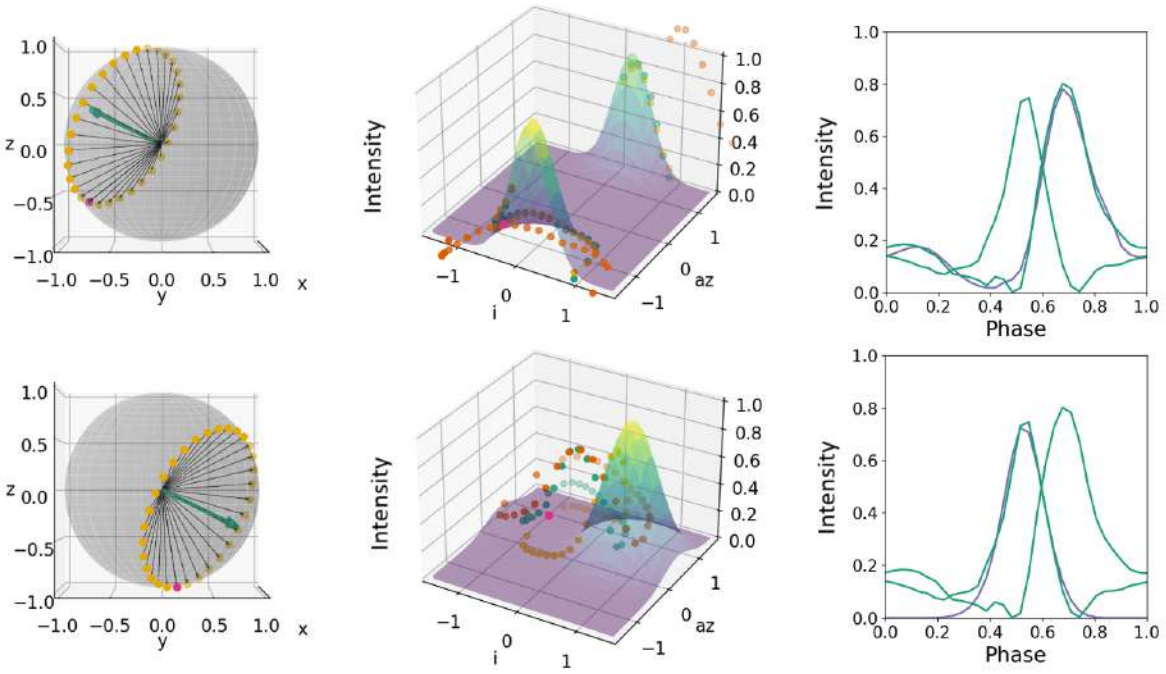

Figure B.21: Same as Figure 3.1 but for the fifth result for Fit 3, right pole (upper panels) and left pole (lower panels). The parameters are listed in Table B.5.

	Result 1	Result 2	Result 3	Result 4	Result 5
	Right pole	Right pole	Right pole	Right pole	Right pole
Rotational inclination (deg)	-19.08	-89.58	4.21	38.32	21.64
Rotational azimuth (deg)	55.88	-106.86	-39.32	85.67	-125.77
Magnetic colatitude (deg)	55.18	19.83	44.16	75.11	60.09
Azimuth shift (rad)	2.08	-1.67	0.59	-0.28	-1.73
Inclination shift (rad)	0.79	0.64	0.55	-0.42	-0.17
Power (-)	3.06	12.16	8.8	5.33	9.46
Neutron star mass ($M_\odot$)	2.97	2.53	2.46	2.54	1.63
Neutron star radius (km)	11.03	11.95	9.38	10.59	9.62
Relative phase shift (rad)	2.54	-0.39	1.41	0.12	0.25
	Left pole	Left pole	Left pole	Left pole	Left pole
Rotational inclination (deg)	19.08	89.58	-4.21	-38.32	-21.64
Rotational azimuth (deg)	-124.12	73.14	140.68	-94.33	54.23
Magnetic colatitude (deg)	52.86	71.6	69.59	30.86	59.96
Azimuth shift (rad)	0.89	0.54	1.2	1.13	-0.41
Inclination shift (rad)	-0.84	2.67	-0.14	0.76	-0.76
Power (-)	8.08	10.54	15.82	14.13	6.71
Neutron star mass ($M_\odot$)	2.97	2.53	2.46	2.54	1.63
Neutron star radius (km)	11.03	11.95	9.38	10.59	9.62
Relative phase shift (rad)	-0.11	0.75	-1.37	2.41	0.06

Table B.5: Table showing all the results obtained when calculating the cost per parameter for Fit 3.

	Result 1	Result 2	Result 3	Result 4	Result 5
Cost	0.10	0.10	0.13	0.088	0.11

Table B.6: The cost obtained for each result when calculating the cost per parameter for Fit 3.

B.2.4. Fit 4

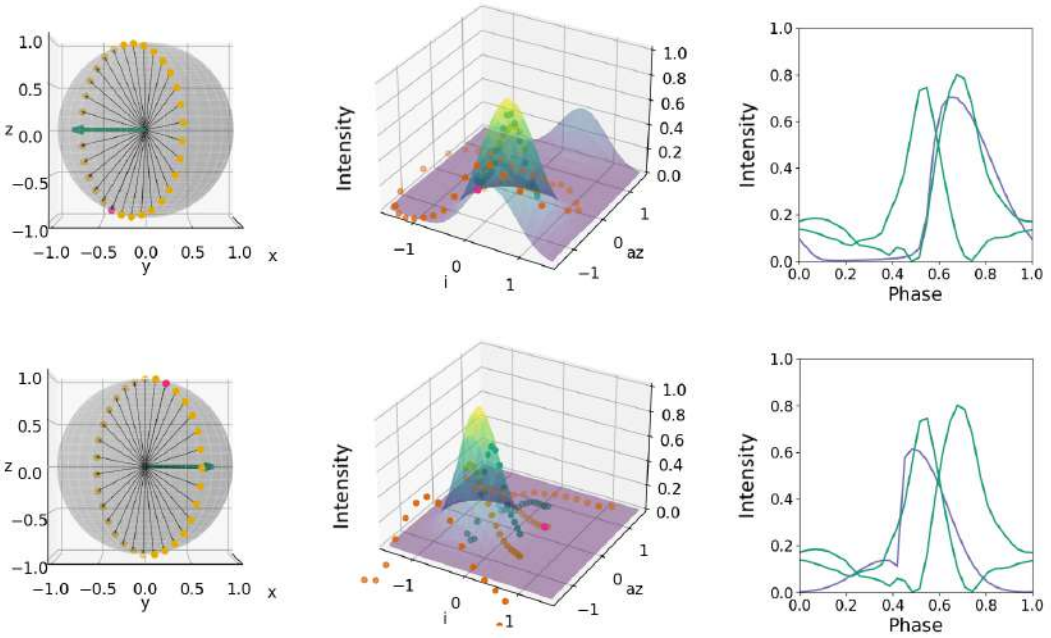

Figure B.22: Same as Figure 3.1 but for the first result for Fit 4, right pole (upper panels) and left pole (lower panels). The parameters are listed in Table B.7.

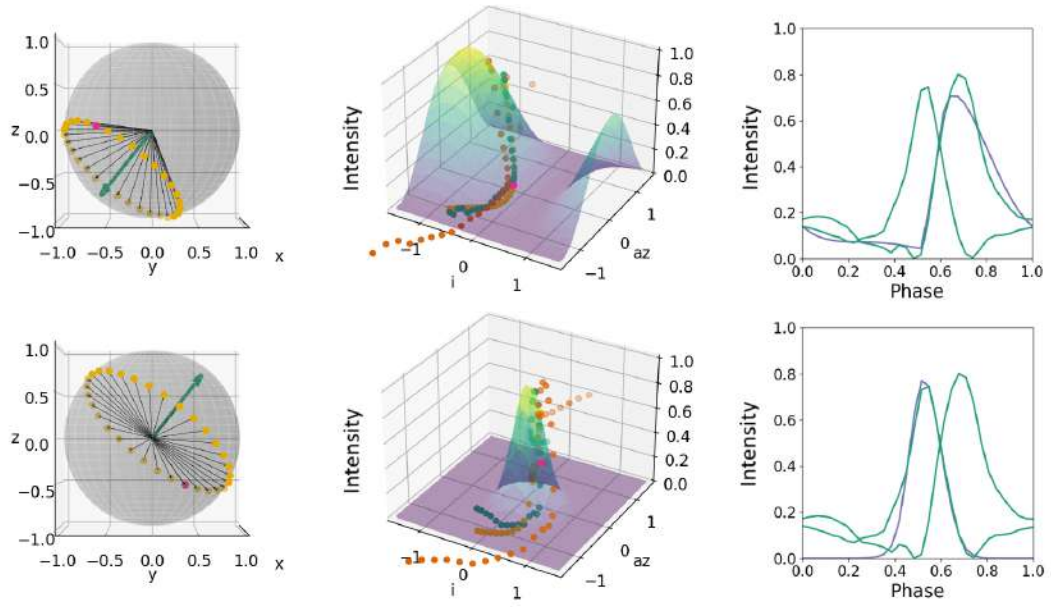

Figure B.23: Same as Figure 3.1 but for the second result for Fit 4, right pole (upper panels) and left pole (lower panels). The parameters are listed in Table B.7.

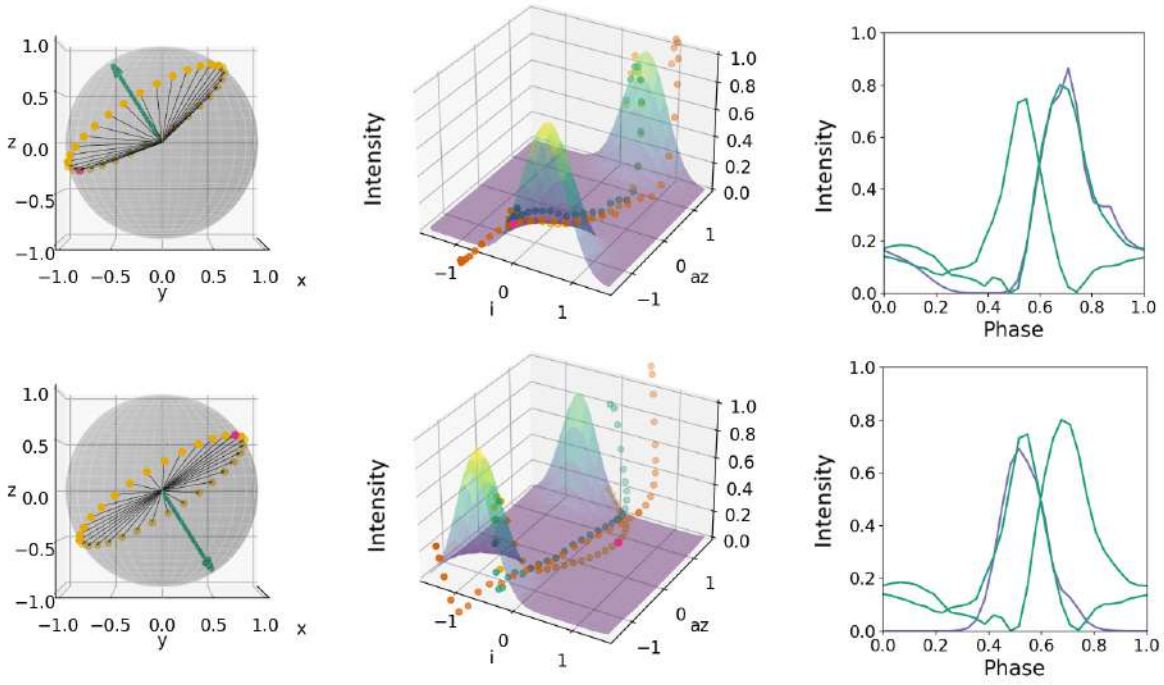

Figure B.24: Same as Figure 3.1 but for the third result for Fit 4, right pole (upper panels) and left pole (lower panels). The parameters are listed in Table B.7.

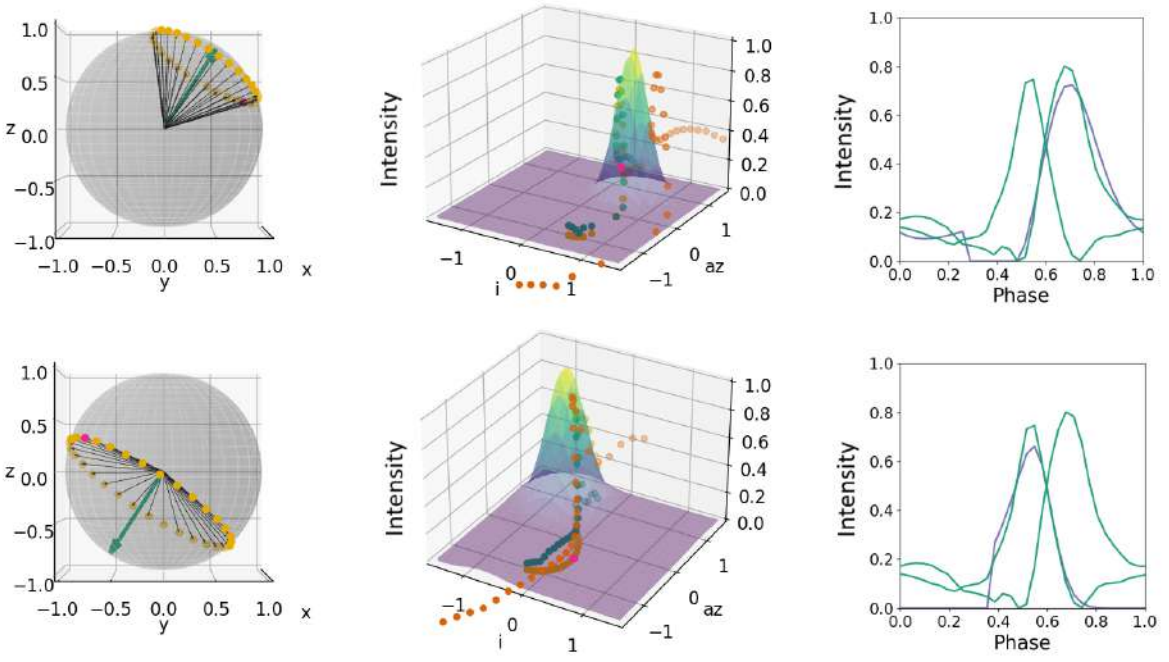

Figure B.25: Same as Figure 3.1 but for the fourth result for Fit 4, right pole (upper panels) and left pole (lower panels). The parameters are listed in Table B.7.

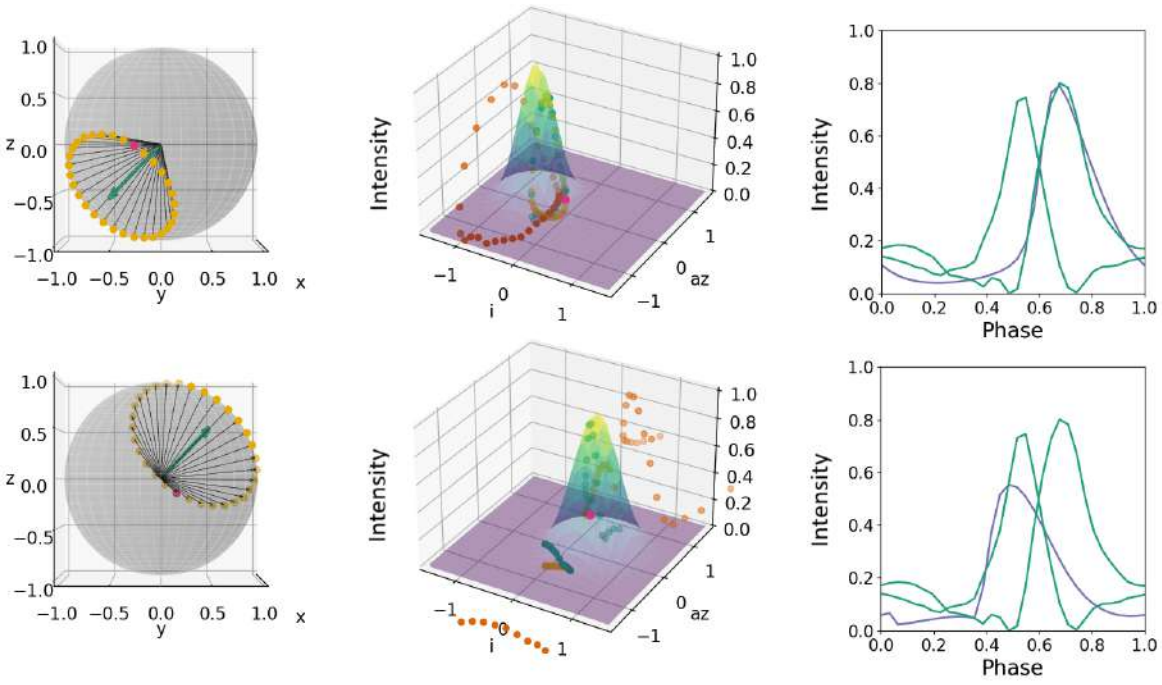

Figure B.26: Same as Figure 3.1 but for the fifth result for Fit 4, right pole (upper panels) and left pole (lower panels). The parameters are listed in Table B.7.

	Result 1	Result 2	Result 3	Result 4	Result 5
	Right pole	Right pole	Right pole	Right pole	Right pole
Rotational inclination (deg)	0.16	-46.99	55.01	54.71	-33.03
Rotational azimuth (deg)	-53.51	-57.56	-114.87	113.21	-38.29
Magnetic colatitude (deg)	77.05	53.12	71.8	39.11	38.79
Azimuth shift (rad)	-2.14	-0.12	-1.72	-0.62	-0.05
Inclination shift (rad)	2.71	1.1	-0.47	2.62	0.58
Power (-)	5.94	2.68	7.76	17.47	12.66
Neutron star mass ($M_\odot$)	2.61	2.46	2.02	2.58	3.0
Neutron star radius (km)	8.88	10.8	11.98	10.47	10.21
Relative phase shift (rad)	-0.37	2.7	-0.01	0.21	2.47
	Left pole	Left pole	Left pole	Left pole	Left pole
Rotational inclination (deg)	-0.16	46.99	-55.01	-54.71	33.03
Rotational azimuth (deg)	126.49	122.44	65.13	-66.79	141.71
Magnetic colatitude (deg)	88.67	84.5	89.87	74.73	49.51
Azimuth shift (rad)	0.39	0.18	1.38	2.29	-0.08
Inclination shift (rad)	0.47	-0.21	0.71	0.72	-0.42
Power (-)	9.56	14.0	9.85	11.12	8.95
Neutron star mass ($M_\odot$)	2.61	2.46	2.02	2.58	3.0
Neutron star radius (km)	8.88	10.8	11.98	10.47	10.21
Relative phase shift (rad)	3.51	0.44	3.16	2.94	0.67

Table B.7: Table showing all the results obtained when calculating the cost per parameter for Fit 4.

	Result 1	Result 2	Result 3	Result 4	Result 5
Cost	0.18	0.13	0.13	0.13	0.16

Table B.8: The cost obtained for each result when calculating the cost per parameter for Fit 4.

Bibliography

[1] W. B. Bonnor, "Jeans' formula for gravitational instability", in: *Monthly Notices of the Royal Astronomical Society* 117.1 (1957), 104–117, DOI: 10.1093/mnras/117.1.104.

[2] Sean G. Ryan and Andrew J. Norton, *Stellar evolution and nucleosynthesis*, Cambridge University Press, 2010.

[3] Megan Watzke and Peter Edmonds, *The secret of magnetic cycles in stars*, 2017, URL: https://www.cfa.harvard.edu/news/secret-magnetic-cycles-stars.

[4] Hannu Karttunen, Pekka KroHERE!HERE!ger, and Heikki Oja, *Fundamental astronomy*, 5th ed., Springer, 2016.

[5] John Daintith and Wiliam Gould, *The Facts on File Dictionary of Astronomy*, 5th ed., Facts on File, 2006.

[6] Andrew Fraknoi, David Morrison, and Sidney C Wolff, *Astronomy 2E*, Openstax, 2022.

[7] A. Heger et al., "How Massive Single Stars End Their Life", in: *The Astrophysical Journal* 591.1 (July 2003), 288–300, ISSN: 1538-4357, DOI: 10.1086/375341, URL: http://dx.doi.org/10.1086/375341.

[8] Werner Becker, *Neutron stars and pulsars*, Springer Berlin Heidelberg, 2009.

[9] Pranab Ghosh, "Properties of Accretion Powered Pulsars", in: *Rotation and Accretion Powered Pulsars*, pp. 413–493, DOI: 10.1142/9789812708465_0009, eprint: https://www.worldscientific.com/doi/pdf/10.1142/9789812708465_0009, URL: https://www.worldscientific.com/doi/abs/10.1142/9789812708465_0009.

[10] Michela Rigoselli, "X-ray observations of isolated neutron stars", in: *Proceedings of Multifrequency Behaviour of High Energy Cosmic Sources XIV — PoS(MULTIF2023)* (2024), DOI: 10.22323/1.447.0055.

[11] Charles W. Misner et al., *Gravitation*, Princeton University Press, 2017.

[12] Andrei M. Beloborodov, "Gravitational Bending of Light Near Compact Objects", in: *The Astrophysical Journal* 566.2 (Feb. 2002), L85–L88, ISSN: 1538-4357, DOI: 10.1086/339511, URL: http://dx.doi.org/10.1086/339511.

[13] Andrew Fraknoi, David Morrison, and Sidney Wolff, *Voyages Through the Universe*, vol. -1, Jan. 2000, ISBN: 0-03-032866-7, DOI: 10.1063/1.882106.

[14] W. Krzeminski, "The Identification and UBV Photometry of the Visible Component of the Centaurus X-3 Binary System", in: 192 (Sept. 1974), p. L135, DOI: 10.1086/181609.

[15] I. Saathoff and A. Santangelo, *Understanding X-ray Pulsars: From Blind Source Separation to Pulse Profile Decompositions*, Universitätsbibliothek Tübingen, 2023, URL: https://books.google.se/books?id=KR4c0AEACAAJ.

[16] Sachindra Naik, Biswajit Paul, and Zulfikar Ali, "X-ray spectroscopy of the high-mass x-ray binary pulsar centaurus x-3 over its binary orbit", in: *The Astrophysical Journal* 737.2 (Aug. 2011), p. 79, ISSN: 1538-4357, DOI: 10.1088/0004-637x/737/2/79, URL: http://dx.doi.org/10.1088/0004-637X/737/2/79.

[17] Juri Poutanen, "Modeling pulse profiles of accreting millisecond pulsars", in: *arXiv: Astrophysics* 1068 (2008), pp. 77–86, URL: https://api.semanticscholar.org/CorpusID:14150072.

TRITA – XXX-XXX 20XX:XX
Stockholm, Sweden 2024

www.kth.se